GEOSPHERE

GEOSPHERE, v. 18, no. 1

https://doi.org/10.1130/GES02417.1

19 figures; 1 table; 1 set of supplemental files

CORRESPONDENCE: jtrop@bucknell.edu

CITATION: Trop, J.M., Benowitz, J.A., Kirby, C.S., and Brueseke, M.E., 2021, Geochronology of the Wrangell Arc: Spatial-temporal evolution of slab-edge magmatism along a flat-slab, subduction-transform transition, Alaska-Yukon: Geosphere, v. 18, no. 1, p. 19–48, https://doi.org/10.1130/GES02417.1.

Science Editor: Shanaka de Silva Guest Associate Editor: David W. Scholl

Received 7 February 2021 Revision received 3 May 2021 Accepted 13 July 2021

Published online 22 December 2021





This paper is published under the terms of the CC-BY-NC license.

© 2021 The Authors

Geochronology of the Wrangell Arc: Spatial-temporal evolution of slab-edge magmatism along a flat-slab, subduction-transform transition, Alaska-Yukon

Jeffrey M. Trop¹, Jeff A. Benowitz², Carl S. Kirby¹, and Matthew E. Brueseke³

ABSTRACT

The Wrangell Arc in Alaska (USA) and adjacent volcanic fields in the Yukon provide a long-term record of interrelations between flat-slab subduction of the Yakutat microplate, strike-slip translation along the Denali-Totschunda-Duke River fault system, and magmatism focused within and proximal to a Cretaceous suture zone. Detrital zircon (DZ) U-Pb (n = 2640) and volcanic lithic (DARL) 40Ar/39Ar dates (n = 2771) from 30 modern river sediment samples document the spatial-temporal evolution of Wrangell Arc magmatism, which includes construction of some of the largest Quaternary volcanoes on Earth. Mismatches in DZ and DARL date distributions highlight the impact of variables such as mineral fertility and downstream mixing/dilution on resulting provenance signatures. Geochronologic data document the initiation of Wrangell Arc magmatism at ca. 30-17 Ma along both sides of the Totschunda fault on the north flank of the Wrangell-St. Elias Mountains in Alaska, followed by southeastward progression of magmatism at ca. 17-10 Ma along the Duke River fault in the Yukon. This spatial-temporal evolution is attributable to dextral translation along intra-arc, strike-slip faults and a change in the geometry of the subducting slab (slab curling/steepening). Magmatism then progressed generally westward outboard of the Totschunda and Duke River faults at ca. 13-6 Ma along the southern flank of the Wrangell-St. Elias Mountains in Alaska and then northwestward from ca. 6 Ma to present in the western Wrangell Mountains. The 13 Ma to present spatial-temporal evolution is consistent with dextral translation along intra-arc, strike-slip faults and previously documented changes in plate boundary conditions, which include an increase in plate convergence rate and angle at ca. 6 Ma. Voluminous magmatism is attributed to shallow subduction-related flux melting and slab edge melting that is driven by asthenospheric upwelling along the lateral edge of the Yakutat flat slab. Magmatism was persistently focused within or adjacent to a remnant suture zone, which indicates that upper plate crustal heterogeneities influenced arc magmatism. Rivers sampled also yield subordinate Paleozoic-Mesozoic DZ and DARL age populations that reflect earlier episodes of magmatism within

underlying accreted terranes and match magmatic flare-ups documented along the Cordilleran margin.

■ INTRODUCTION

Junctions between magmatic arcs and transform margins are a fundamental feature of modern and ancient plate tectonics (e.g., Wakabayashi, 1996; Maury et al., 2004; Harrison et al., 2004; Cooper et al., 2010; Wang et al., 2009). Many active volcanic arcs transition laterally into transform margins in diverse oceanic settings (Kamchatka, Portnyagin et al., 2005; South Philippine Sea, Fitch, 1972; New Zealand, Lebrun et al., 2000; Papua New Guinea, Baldwin et al., 2012; Southern Patagonia, Polonia et al., 2007; East Scotia Sea, Leat et al., 2004; Tonga, Cooper et al., 2010). Compared to oceanic settings, active arc-transform junctions are less common in continental settings with notable examples in eastern Alaska (Wrangell Arc, Brueseke et al., 2019), Myanmar (Lee et al., 2016), and Cyprus-Turkey (Symeou et al., 2018).

Arc-transform junctions exhibit complex spatial transitions from typical subduction-related arc magmatism to upwelling of asthenosphere along subducting slab edges, tears, windows, and transform faults (e.g., Park et al., 2002; Leat et al., 2004; Thorkelson et al., 2011; Lee et al., 2016; Grebennikov and Khanchuk, 2020). Active arc-transform junctions offer a unique geological record of both convergent and transform margin processes, yet the nature of such junctions and their influence on the evolution of orogenic belts is seldom discussed in the literature.

Subhorizontal (flat) subduction has shaped numerous modern and ancient plate margins (e.g., Gutscher et al., 2000; Lawton, 2008; Kapp and DeCelles, 2019). Slab flattening has been attributed to the subduction of buoyant oceanic lithosphere, rapid trenchward progression of the overriding plate, and mantle wedge dynamic pressure (slab suction) (e.g., Kay and Mpodozis, 2002; Guillaume et al., 2009; Martinod et al., 2010; Schellart, 2020). Slab flattening induces upper plate compressional stresses that prompt intensification and inboard progression of upper plate shortening, exhumation, and sediment accumulation (e.g., Fan and Carrapa, 2014; Stevens Goddard and Carrapa,

Jeffrey M. Trop https://orcid.org/0000-0002-2068-0037

Department of Geology and Environmental Geosciences, Bucknell University, Lewisburg, Pennsylvania 17837, USA

²Department of Geosciences, University of Alaska, Fairbanks, Alaska 99775, USA

³Department of Geology, Kansas State University, 108 Thompson Hall, Manhattan, Kansas 66506, USA

2018; Capaldi et al., 2020) and can drive continental strike-slip fault motion (Giambiagi et al., 2017). Arc magmatism often shifts inboard and wanes or ceases in response to inboard progression of the locus of dehydration melting above the hinge of the subducting flat slab and displacement of lower continental mantle lithosphere into the asthenospheric wedge (e.g., Bishop et al., 2017; Schellart, 2017; Axen et al., 2018). Whereas recent studies elucidated processes that shape the medial portions of overriding plates above subducted flat slabs, time-space studies from the lateral margins (edges) of flattened slabs are generally lacking.

The Yakutat microplate is actively colliding and subducting shallowly (i.e., flat-slab subduction, though we recognize here that the sub-horizontal portion of the slab dips at an angle of ~20° and thus is not truly "flat") beneath south-central Alaska and adjacent to a complex tectonic corner. The corner, referred to as the St. Elias syntaxis, marks a west-to-east transition from chiefly collision and flat-slab subduction of the Yakutat microplate to strain-partitioned, strike-slip deformation along transform faults (Fig. 1; Pavlis et al., 2019). Recent research provides insight into processes within and outboard (south) of the collision zone (e.g., Enkelmann et al., 2015a, 2015b; Gulick et al., 2015; Bootes et al., 2019; Schartman et al., 2019). Inboard of the collision zone, the Wrangell Arc spans the transitional position between flat-slab subduction of the Yakutat microplate and transform tectonics along the continental margin of western North America (Fig. 1). Wrangell Arc eruptive centers are superbly exposed where they are not covered by glacial ice, largely undeformed, and imaged with modern geophysical techniques, which thus makes the region a prime locale to study magmatism over a flat-slab transform environ.

This study quantifies the temporal and spatial evolution of Wrangell Arc magmatism and evaluates the role of tectonic processes and structures on magmatism. We present abundant new detrital zircon (DZ) U-Pb and detrital volcanic lithic (DARL) 40Ar/39Ar dates from modern river sediment samples and integrate these results with existing and new igneous bedrock geochrononologic data. The new dates also better quantify Mesozoic–Paleozoic magmatism that shaped the lithosphere prior to Wrangell Arc magmatism. Collectively, new DZ and DARL data reveal persistent magmatism since 30 Ma within a remnant suture zone and spatial changes in the location of magmatism that are interpreted to reflect changes in plate interactions and dextral translation of the overriding plate along regional strike-slip faults spanning the arc-transform junction.

More broadly, the present study highlights the utility of multi-proxy methods in sedimentary sinks located proximal to magmatic arc sources. Detrital zircon U-Pb geochronology has become a fundamental, widely used provenance tool in reconstructing sedimentary provenance, sediment dispersal pathways, and geologic/tectonic histories (e.g., Cawood et al., 2012; Gehrels, 2014). Despite the widespread utility of DZ data, there are limitations in interpreting sediment provenance from DZ. For example, detrital contributions may not be proportional to source unit exposure area due to heterogeneous zircon fertility among bedrock sources (e.g., Dickinson, 2008; Malusà et al., 2016; Spencer et al., 2018), irregular bedrock erodibility (Capaldi et al., 2017), and

variable lithologic breakdown by weathering, erosion, and climate (Amidon et al., 2005). In the present study, differences between DZ and DARL dates highlight the utility of the combined techniques for deciphering the evolution of magmatic provinces.

■ REGIONAL TECTONIC SETTING

The northern Pacific plate margin is characterized by a west-to-east transition from typical subduction to flat-slab subduction to transform tectonics. Along-strike variations in seismicity and volcanism indicate two subducting plates with varying dip angles (e.g., Li et al., 2016; Yang and Gao, 2020). In the western region, northwesterly subduction of the Pacific plate beneath the North American plate along the Aleutian megathrust produces a well-defined trench, moderately dipping slab (~40°) that reaches depths of 100–150 km within ~400 km of the trench, and linear Aleutian volcanoes that are attributed to subducted-related arc magmatism (Jicha et al., 2006; Syracuse and Abers, 2006; Nye et al., 2018). Aleutian arc volcanoes are chiefly stratovolcanoes with increasing arc-trench distance from southwest to northeast along strike (Fig. 1; Miller et al., 1998).

The central region is distinguished by a shallowly dipping slab resulting from collision and relatively flat subduction of the Yakutat microplate. The Yakutat microplate is a 15–30-km-thick oceanic plateau that thins inboard (northwestward) (Worthington et al., 2012). A subducted Yakutat slab extends subhorizontally ("flat") for ~250 km northwestward beneath Alaska at a subduction angle of ~6° before dip angle increases to ~20° and reaches a depth of 150 km >600 km inboard of the Aleutian trench (Fig. 1; Eberhart-Phillips et al., 2006). The Pleistocene–Holocene Buzzard Creek-Jumbo Dome volcanoes, which are much smaller than the Aleutian arc volcanoes, occur along the northern edge of the subducted slab (JD and BM in Fig. 1) and reflect subducted-related continental arc magmatism (Albanese, 1980; Andronikov and Mukasa, 2010; Nye et al., 2018). A region with no active volcanism, referred to as the Denali volcanic gap, separates the Aleutian arc and the Buzzard Creek-Jumbo Dome volcanoes (Fig. 1; Rondenay et al., 2010).

The eastern region, the focus of this study, is a tectonic corner where the plate margin transitions from fully convergent to a transpressional transform system (Schartman et al., 2019). Deformation transitions from an east-west-trending, fold-thrust belt above the colliding Yakutat microplate to a system of northwest-trending, strike-slip faults along the eastern edge of the terrane (Fig. 1; Pavlis et al., 2019). The dominantly strike-slip Fairweather fault accommodates dextral motion of the Yakutat microplate relative to North America (Figs. 1 and 2). Right lateral shear is currently transferred inboard to the central Denali fault via the Totschunda fault and perhaps via an inferred Connector fault (Figs. 1 and 2; Haeussler et al., 2017; Marechal et al., 2018). Along the northern, inboard margin of the tectonic corner, the edge of the subducted Yakutat microplate dips northerly from ~11° to ~16° and projects to ~80 km beneath clustered volcanoes comprising the Wrangell Arc (Bauer et al., 2014).

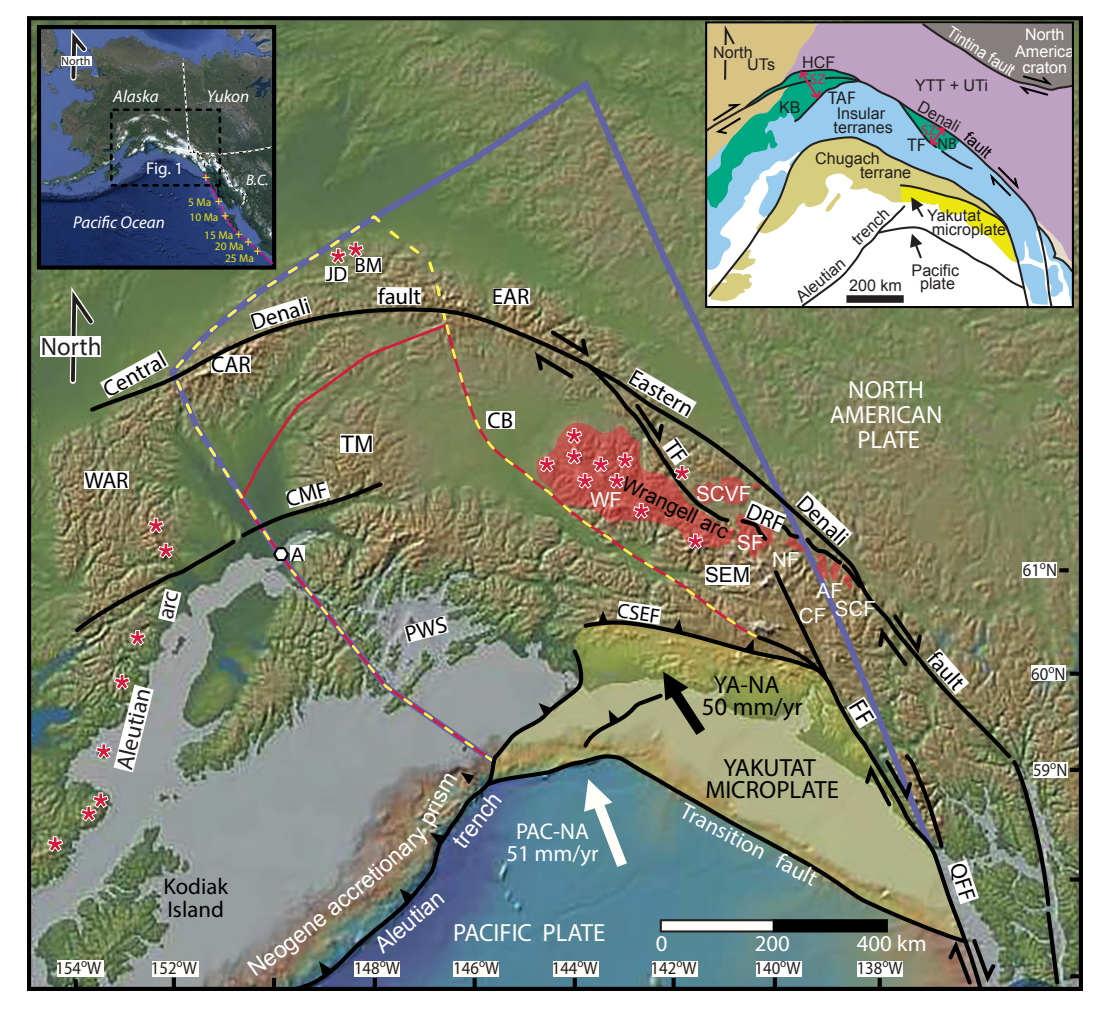


Figure 1. Tectonic framework of southern Alaska, the Yukon, and coastal British Columbia shows regional faults with known or suspected Neogene and younger displacement (from Plafker et al., 1994; Koehler et al., 2012; Yukon Geological Survey, 2020), exposed (light yellow) and interpreted subducted extent (region within bold dashed yellow line) of the Yakutat microplate and volcanic fields comprising the Wrangell Arc (transparent red) in Alaska (SCVF—Sonya Creek field, WF—Wrangell field) and Canada (AF—Alsek field, NF—Nines Creek field, SF—St. Clare field) including <5 Ma volcanoes denoted by red asterisks (Cameron, 2005). Solid red line denotes the region of flat-slab subduction of Yakutat microplate. Yellow line denotes loosely constrained edge of subducted Yakutat microplate based chiefly on tomography data (adapted from Eberhart-Phillips et al., 2006). Blue line denotes loosely constrained edge of subducted Yakutat microplate based chiefly on plate kinematics (adapted from Pavlis et al., 2019). Dashed magenta curve in index map in upper left shows Fairweather–Transition–Queen Charlotte fault intersection triple junction track during the past 25 m.y. (from Pavlis et al., 2019, using Doubrovine and Tarduno, 2008, plate model). Yellow crosses show Fairweather–Transition–Queen Charlotte triple junction location at time points. Inset at upper right shows Cretaceous suture zone separating Insular terranes from inboard terranes. Abbreviations: A—Anchorage, B.C.—British Columbia, BM—Buzzard Creek maar, CAR—central Alaska Range, CB—Copper River basin, CF—Connector fault (inferred), CMF—Castle Mountain fault, CSEF—Chugach-St. Elias fault, DRF—Duke River fault, EAR—eastern Alaska Range, FF—Fairweather fault, HCF—Hines Creek fault, JD—Jumbo Dome volcano, KB—Kahiltna basin, NB—Nutzotin basin, QFF—Queen-Charlotte-Fairweather fault, PWS—Prince William Sound, SEM—St. Elias Mountains, TAF—Talkeetna Mountains, TF—Totschunda fault, UTi—undifferentiated terranes and sedimentary rocks, WAR—western Alaska Range, WF—Wrangell volca

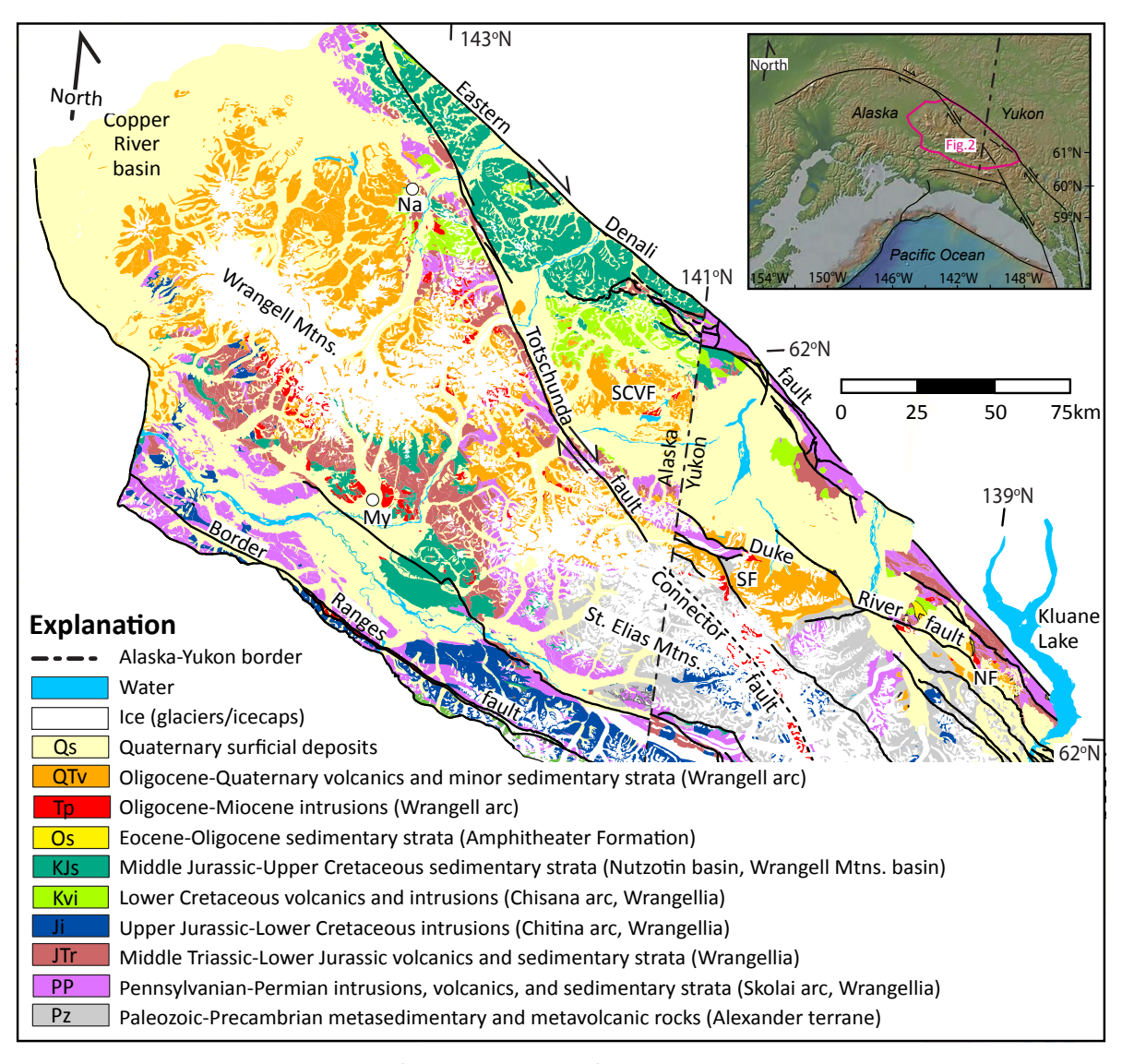
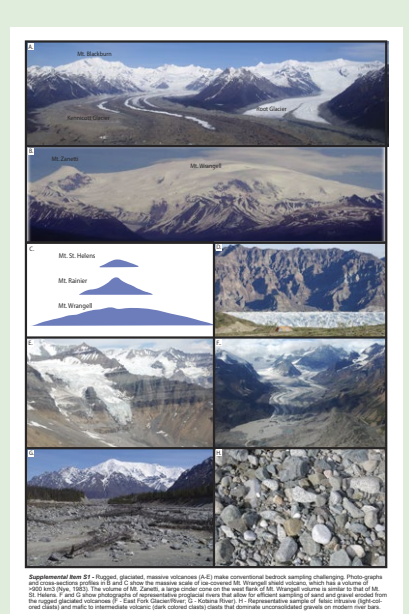


Figure 2. Geological map shows the Wrangell Arc (orange and red polygons) and older bedrock in the Wrangell–St. Elias Mountains of eastern Alaska and the Yukon. Orange polygons show Wrangell Arc volcanics, which include the Wrangell volcanic field (large field southwest of the Totschunda fault) and smaller fields to the east (NF—Nines Creek field, SCVF—Sonya Creek field, SF—St. Clare field, Na - town of Nabesna, My - town of McCarthy). Inset at upper right shows map location (pink polygon); refer to Figure 1 for additional location information. Geology is from Richter et al. (2006), Wilson et al. (2015), and Yukon Geological Survey (2020).



¹Supplemental Material, Item S1: Physiographic aspects of the Wrangell Arc that make bedrock sampling challenging, including scale of eruptive centers and glaciated, rugged, roadless terrain. Item S2: Photomicrographs of representative sand samples from modern rivers showing abundant volcanic lithic grains. Item S3: Modern river sediment sample location information. Item S4: Methods for calculating watershed boundaries, surface area of ice, surficial deposits, and bedrock, and geochronologic samples. Item S5: Summary of surface area of ice, surficial deposits, and bedrock within sampled watersheds. Item S6: 40 Ar/39 Ar and U-Pb analytical details. Item S7: New igneous bedrock 40Ar/39Ar fusion data. Item S8: Previously reported igneous bedrock data. Item S9: Detrital cobble-sized 40Ar/39Ar (DARL) fusion data. Item S10: Detrital sand-sized 40Ar/39Ar (DARL) step-heat data. Item S11: Detrital sand-sized volcanic-lithic 40Ar/39Ar (DARL) fusion data. Item S12: Detrital zircon (DZ) U-Pb age data. Item S13: Examples of differences between detrital zircon (DZ) vs. volcanic lithic (DARL) dates. Please visit https://doi.org/10.1130/GEOS.S.15167367 to access the supplemental material, and contact editing@geosociety.org with any questions.

■ WRANGELL ARC

The Wrangell volcanic belt consists of a >450-km-long and up to 190-km-wide belt of ca. 30 Ma to 1500 ka volcanoes in the Wrangell–St. Elias Mountains in eastern Alaska, southwestern Yukon, and northwestern British Columbia (Figs. 1–2). Wrangell Arc eruptive centers occur within and immediately outboard (south) of a Cretaceous suture zone that separates the accreted Insular terranes from older terranes exposed inboard (northeast) of the Denali fault (Figs. 1–2).

Wrangell volcanic belt lavas, domes, and pyroclastic deposits erupted from large shield volcanoes and subordinate stratovolcanoes, caldera complexes, and scoria cones after ca. 30 Ma (Figs. 1–3 and Item S1 in the Supplemental Material¹; Richter et al., 1990, 2006; Brueseke et al., 2019). Previously reported geochronological data consist chiefly of whole rock K-Ar dates and subordinate whole rock and single crystal U-Pb and ⁴⁰Ar/³⁹Ar dates; vast, ice-covered areas lack geochronologic data.

At least six volcanic fields make up the belt: the Wrangell, Sonya Creek, St. Clare, Nines Creek, Alsek, and Stanley Creek fields (Fig. 1). The largest of the fields, the Wrangell field in Alaska (WF in Fig. 1), reflects subduction-related arc magmatism and slab-edge upwelling of asthenosphere based on transitional to calc-alkaline geochemical compositions (Preece and Hart, 2004; Brueseke et al., 2019) and the spatial association of Quaternary shield and stratovolcanoes above a geophysically imaged, northeastward-dipping subducting slab along the northeastern edge of the Yakutat microplate (Bauer et al., 2014). Geochemical spatial trends in <5 Ma volcanoes in the western Wrangell field are consistent with north-dipping subduction, including calc-alkaline to tholeitic suites related to intra-arc extension within the interior and northern back-side of the Wrangell Arc, a calc-alkaline suite that crops out throughout the arc, and a calc-alkaline adakitic suite found only along the front-side of the arc during this time period.

In the eastern part of the Wrangell field, 13–5 Ma calc-alkaline to tholeiitic lavas, pyroclastic deposits, shallow intrusives, and sedimentary strata record intra-arc transtensional basin development attributed to subduction of oceanic lithosphere of the Yakutat microplate and strike-slip deformation (Trop et al., 2012). The Sonya Creek field (SCVF in Figs. 1–2), located immediately west of the Yukon-Alaska border, comprises ca. 30–19 Ma calc-alkaline, transitional-tholeiitic, and adakite-like, volcanic-intrusive suites and represents the earliest phase of arc magmatism related to subduction of Yakutat microplate oceanic lithosphere beneath North America (Berkelhammer et al., 2019; Brueseke et al., 2019).

In Canada, four volcanic fields composed of Miocene lavas, pyroclastic rocks, and intrusions crop out for >300 km along the Duke River fault (AF, SF, SCF, and NF in Fig. 1). The St. Clare field consists of 18–10 Ma transitional and minor alkaline and calc-alkaline lavas, and 16–13 Ma transitional lavas make up the Nines Creek field (Skulski et al., 1992). The Alsek field consists of 14–11 Ma calc-alkaline and minor transitional and alkaline lavas (Dodds and Campbell, 1988), whereas transitional and minor alkaline lavas make up the Stanley Creek field (Skulski et al., 1991). Wrangell Arc volcanic fields in Canada are interpreted as the product of both subduction-related arc magmatism and

intraplate-type magmatism; eruptions occurred along strike-slip faults judging from geochemical compositions and the close spatial association of volcanoes and strike-slip faults (Skulski et al., 1992; Thorkelson et al., 2011).

In summary, the Wrangell and Sonya Creek fields in Alaska record subduction-related arc volcanism and are thus referred to as the Wrangell Arc, whereas volcanic fields in Canada record both subduction-related arc magmatism and magmatism sourced from mantle unaffected by arc processes. Magmatic products in both Canada and Alaska erupted along "leaky" strike-slip faults that were active conduits for magma ascent.

METHODS

Modern river detrital geochronology and targeted bedrock dating was used to maximize spatial coverage and access material eroded beneath glacial ice. Modern river bars composed of unconsolidated sand and gravel were sampled from 22 transverse rivers and eight tributaries (Fig. 3, Table 1, and Items S2-S3 [see footnote 1]). Sand and cobble fractions were sampled for detrital zircon and volcanic lithic geochronology. Unlike detrital minerals such as zircon, dates from volcanic lithics provide direct lithologic information about the volcanic source region. Dating of volcanic lithics also addresses mineral fertility concerns associated with zircon-poor mafic to intermediate composition igneous rocks that are common in the study area (Richter et al., 2006). At each sample site, a petrological survey of the cobble fraction was completed prior to sampling cobbles that are representative of all observed igneous lithologies; ~15-20 cobbles were sampled per site for companion geochemical analyses. Individual cobbles were then split by hammer and prepared for 40Ar/39Ar geochronologic analyses (DARL) and wavelength dispersive X-ray fluorescence (XRF) geochemical analyses (refer to Morter, 2017, for XRF results). From the same river bars, several kilograms of sand were collected for U-Pb geochronology on sand-sized DZ grains and 40Ar/39Ar geochronology on sand-sized DARL grains. Bedrock samples were also collected from some previously unsampled portions of the study region to provide a framework to compare more abundant and inclusive detrital dates from modern river sediments reported herein.

ArcMap Geographic Information System (GIS) software was used to plot sample locations, delineate watershed areas upslope of detrital samples, and calculate the areal extent of ice, surficial deposits, and bedrock units within the watersheds sampled. Refer to Items S4–S5 (footnote 1) for GIS methods and results.

⁴⁰Ar/³⁸Ar geochronologic analyses were carried out at the University of Alaska Fairbanks Geochronology Lab using the single grain and multi-grain fusion method to optimize the number of samples versus the precision and full isotopic evaluation that step-heating analysis allows. The new fusion (total gas) data yield uncertainties comparable to legacy K-Ar data reported from the Wrangell Arc. U-Pb geochronology was carried out on zircon grains by Laser Ablation-Inductively Coupled Plasma-Mass Spectrometry (LA-ICP-MS) at the University of Arizona LaserChron Center. Refer to Items S6–S12 (footnote 1) for full ⁴⁰Ar/³⁹Ar and U-Pb analytical details and results.

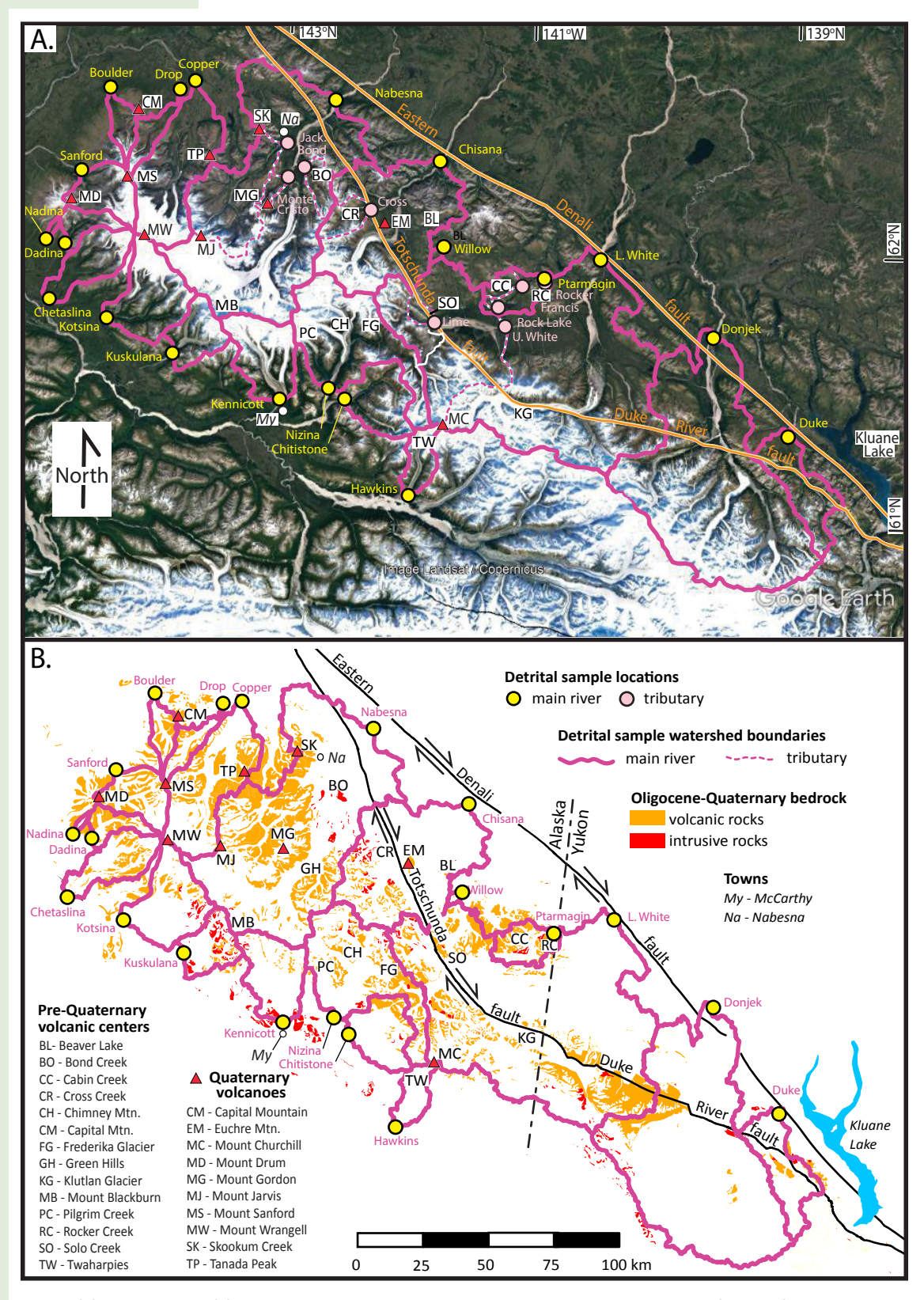


Figure 3. (A) Google Earth and (B) geologic map show watershed boundaries upslope of modern river samples (pink lines), exposed Wrangell Arc volcanics (orange polygons) and intrusions (red polygons), and regional strike-slip faults (black lines). Note ice (white in B) making up 29% of the surface area of the sampled watersheds. Refer to Figures 2 and Item S5 (text footnote 1) for location and additional geologic context.

TABLE 1. SUMMARY OF DETRITAL DATES FROM MODERN RIVERS DRAINING THE WRANGELL ARC, WRANGELL-ST. ELIAS MOUNTAINS, ALASKA-CANADA

Catchment name	e Catchment type	Latitude	Longitude	Detrital zircon (DZ) U-Pb dates			Detrital 40Ar/39Ar volcanic lithics (DARL) (sand-sized)			Detrital ⁴⁰ Ar/ ³⁹ Ar volcanic lithics (DARL) (cobble-sized)					
				n _{total}	n _{<35 Ma}	% _{<35 Ma}	n _{total}	n _{<35 Ma}	% _{<35 Ma}	n _{total}	n _{<35 Ma}	% _{<35 Ma}	n _{total}	n _{<35 Ma}	% _{<35 N}
Northeastern Wa	atershed														
Francis	Tributary (Ptarmagin)	N61°52′16.47"	W141°09′21.22″	n/a	n/a	n/a	113	111	98	n/a	n/a	n/a	113	111	98
Rocker	Tributary (Ptarmagin)	N61°48'25.60"	W141°18'43.39"	299	3	1	119	83	70	n/a	n/a	n/a	418	86	21
Rock Lake	Tributary (Ptarmagin)	N62°54'46.08"	W141°03′43.22"	n/a	n/a	n/a	37	33	89	n/a	n/a	n/a	37	33	89
Ptarmagin	Main River	N61°54'48.99"	W141°04′15.21"	309	29	9	108	107	99	n/a	n/a	n/a	417	136	33
Willow	Main River	N62°00′18.61″	W141°44'30.73"	n/a	n/a	n/a	28	14	50	n/a	n/a	n/a	28	14	50
Cross	Tributary (Chisana)	N62°07′56.29"	W142°18′11.36"	n/a	n/a	n/a	115	20	17	11	4	36	126	24	19
Chisana	Main River	N62°11'25.09"	W142°05'45.75"	56	6	11	110	49	45	19	17	89	185	72	39
Totals/Means				664	38	6	630	417	66	30	21	70	1324	476	36
Eastern															
Duke River	Main River	N61°22'32.54"	W139°08'40.41"	290	10	3	n/a	n/a	n/a	n/a	n/a	n/a	290	10	3
Donjek	Main River	N61°40'46.14"	W139°45'02.09"	297	21	7	n/a	n/a	n/a	n/a	n/a	n/a	297	21	7
Lime	Tributary (U. White)	N62°45'25.60"	W141°49′56.50″	n/a	n/a	n/a	101	29	29	n/a	n/a	n/a	101	29	29
Upper White	Tributary (L. White)	N61°43'37.94"	W141°17′15.88″	308	63	20	120	77	64	14	10	71	442	150	34
Lower White	Main River	N61°59′15.80″	W140°33′ 29.03″	291	133	46	n/a	n/a	n/a	n/a	n/a	n/a	291	133	46
Totals/Means				1186	227	19	221	106	48	0 14	10	71	1421	343	24
Southern															
Kuskulana	Main River	N61°36′42.48″	W143°42′29.72″	86	86	100	109	78	72	16	16	100	211	180	85
Kotsina	Main River	N61°42′58.03″	W144°16′52.77″	26	15	58	109	85	78	13	10	77	148	110	74
Kennicott	Main River	N61°26′02.36″	W142°56′26.90″	145	123	85	111	72	65	n/a	n/a	n/a	256	195	76
Nizina	Main River	N61°29′30.03″	W142°34′32.95″	305	51	17	105	52	50	n/a	n/a	n/a	410	103	25
Chitistone	Main River	N61°27′35.26″	W142°28′26.69″	257	160	62	94	37	39	n/a	n/a	n/a	351	197	56
Hawkins	Main River	N61°08′36.73″	W142°03′10.52″	279	235	84	108	37	34	n/a	n/a	n/a	387	272	70
Totals/Means				1098	670	61	636	361	57	29	26	90	1763	1057	60
North Central															
Jacksina Jacksina	Tributary (Nabesna)	N62°21′36.70″	W142°57′13.10″	n/a	n/a	n/a	115	114	99	n/a	n/a	n/a	115	114	99
Monte Cristo	Tributary (Nabesna)	N62°13'26.97"	W142°55′30.73″	n/a	n/a	n/a	100	93	93	n/a	n/a	n/a	100	93	93
Bond	Tributary (Nabesna)	N62°16′26.10″	W142°51′00.00″	n/a	n/a	n/a	108	13	12	n/a	n/a	n/a	108	13	12
Nabesna	Main River	N62°25′22.27"	W142°47′46.93″	107	6	6	119	112	94	12	10	83	238	128	54
Totals/Means				107	6	6	442	332	75	12	10	83	561	348	62
Northwestern															
Copper	Main River	N62°34′06.10″	W143°41′48.80″	77	60	78	101	101	100	n/a	n/a	n/a	178	161	90
Drop	Main River	N62°32′14.00″	W143°47′31.70″	251	234	93	110	110	100	n/a	n/a	n/a	361	344	95
Boulder	Main River	N62°31′42.50″	W144°21′54.10″	122	34	28	48	48	100	n/a	n/a	n/a	170	82	48
Sanford	Main River	N62°11′06.16″	W144°29′54.45″	158	30	19	117	117	100	18	18	100	293	165	56
Nadina (east)	Main River	N61°58′35.97″	W144°44′48.67″	84	81	96	n/a	n/a	n/a	n/a	n/a	n/a	84	81	96
Nadina (west)	Main River	N62°00′27.24″	W144°32′33.60″	n/a	n/a	n/a	n/a	n/a	n/a	8	8	100	8	8	100
Dadina (11001)	Main River	N61°57′29.60″	W144°40′12.44″	83	5	6	114	114	100	11	11	100	208	130	63
Chetaslina	Main River	N62°45′02.66″	W144°41′01.92″	110	0	0	221	212	96	9	7	78	340	219	64
Totals/Means				885	444	50	711	702	99	46	44	96	1642	1190	72
Total				3940	1385	35	2640	1918	73	131	111	85	6711	3414	51

Summary of New Bedrock Dates

This study reports a total of 61 new single grain fusion and multi-grain fusion bedrock ⁴⁰Ar/³⁹Ar groundmass dates (Item S7 [footnote 1]). These dates both confirm and supplement previously published bedrock dates (n = 348; Item S8). New bedrock dates document magmatism between 30 Ma and <1 Ma among the sampled watersheds and are consistent with previous bedrock dates reported from the Wrangell Arc (Item S8). These new bedrock dates are integrated with abundant new detrital dates that are presented below in the Discussion.

Summary of Modern River Sediment Detrital Dates

This study reports a total of 3940 sand-sized DZ U-Pb, 2640 sand-sized DARL ⁴⁰Ar/³⁹Ar, and 131 cobble-sized DARL ⁴⁰Ar/³⁹Ar dates from modern sediment from 22 major rivers and eight tributaries. Figure 4 summarizes the geology with the watersheds that were sampled. Figures 5–9 display relative age probability plots of modern river sediment samples. Figures 10–12 display composite probability plots of all samples. Figures 13–15 show the spatial distribution of <35 Ma detrital dates. The following sections summarize key age results from the overall study region followed by age patterns from five sub-regions.

Detrital dates (n = 6711) from the modern rivers sampled are chiefly Cenozoic (58% of total age population) with subordinate Mesozoic (25%), Paleozoic (15%), and Precambrian (2%) populations. Detrital dates of <35 Ma compose the dominant age population, comprising 51% of all detrital dates, including 35% of DZ dates, 73% of sand-sized DARL dates, and 85% of cobble-sized DARL dates (Table 1). Ages of <35 Ma make up the dominant age population of 19 of 30 sand-sized DARL samples, nine of 10 cobble DARL samples, and eight of 21 DZ samples. For sediment samples with both DZ and DARL dates, 14 of 17 rivers yield a higher proportion of <35 Ma DARL dates than <35 Ma DZ dates. Subordinate detrital populations are >320 Ma (4%), 320–270 Ma (early Pennsylvanian–Early Permian; 12% of total population), 270–220 Ma (Late Permian–Late Triassic; 2%), 220–160 Ma (Late Triassic–Late Jurassic; 4%), 160–130 Ma (Early Cretaceous–Late Jurassic; 9%), 130–110 Ma (Early Cretaceous; 5%), 90–50 Ma (early Eocene–Late Cretaceous; 10%), and 50–35 Ma (Paleogene; 0.6%).

Spatial Variations in Modern River Detrital Dates

Northeastern Rivers

Modern river sediment samples along the northeastern flank of the Wrangell–St. Elias Mountains show abundant Cenozoic (60%) detrital dates and subordinate Mesozoic (37%), Paleozoic (2%), and Precambrian (1%) detrital dates (n = 1421) (Figs. 5, 10 and Items S9–S12 [footnote 1]). Detrital

dates >35 Ma include three main populations: 235–185 Ma (Triassic–Jurassic), 118–100 Ma (Early Cretaceous), and 70–58 Ma (Late Cretaceous–Paleogene). Detrital dates >35 Ma are substantially more common within the DZ sand fraction (94%) than in the DARL sand fraction (44%). Detrital dates <35 Ma represent 36% of all detrital dates, including ~6% of DZ dates, ~66% of sand-sized DARL dates, and ~70% of cobble-sized DARL dates (Table 1). Seven rivers yield dominant apparent age peaks between 17 Ma and 35 Ma, whereas three rivers show dominant apparent age peaks that fall between 6 Ma and 13 Ma (Fig. 5).

Detrital dates from northeastern river sediment samples overlap with <35 Ma bedrock dates reported from their watersheds, although some detrital dates are not present in the available bedrock data (Fig. 5). Samples from the Ptarmigan, Francis, Willow, and Rock Lake drainages yield dominant detrital age populations between 17 Ma and 35 Ma that match bedrock dates reported from their watersheds. Samples from the Chisana and Cross drainages show detrital dates between 17 Ma and 35 Ma and 1 Ma to 3 Ma that correspond with bedrock dates from those watersheds. However, the Chisana and Cross samples also yield 13–17 Ma and 6–8 Ma detrital dates that are not present among the available bedrock dates within their watersheds.

Eastern Rivers

Modern sediment samples from five watersheds spanning the Alaska-Yukon border reveal Cenozoic (28%), Mesozoic (11%), Paleozoic (54%), and Precambrian (7%) detrital dates (n = 1421) (Figs. 6, 10, and Items S9–S12 [footnote 1]). Detrital dates >35 Ma comprise five main populations between 65 Ma and 54 Ma (Paleogene), 127–110 Ma (Cretaceous), 312–271 Ma (Pennsylvanian–Permian), 2110–1710 Ma (Proterozoic), and 2840–2460 Ma (Proterozoic–Archean). The Duke, Donjek, and Lower White Rivers yield the majority of Proterozoic detrital dates. Detrital dates >35 Ma are more common in the DZ sand fraction (81%) than in the DARL sand fraction (52%). Dates of <35 Ma comprise 24% of the total age population in eastern river samples. Samples from the Upper White, Lower White, and Donjek drainages yield dominant DZ populations between 8 Ma and 13 Ma, whereas samples from the Duke drainage show dominant DZ populations between 17 Ma and 35 Ma. Samples from the Lime and Upper White drainages show dominant DARL populations between 17 Ma and 35 Ma and 8 Ma to 13 Ma, respectively.

Detrital dates from eastern sediment samples broadly correspond with 8–35 Ma bedrock dates reported from their watersheds. Dominant detrital age populations between 17 Ma and 35 Ma and 13 Ma to 11 Ma in the Lime and Upper White samples match dominant bedrock dates reported from those watersheds. However, minor populations of <11 Ma detrital dates from those drainages are not present in the available bedrock data. Detrital dates in samples from the Lower White, Duke, and Donjek Rivers match bedrock dates in spatially associated watersheds. However, sparse 17–35 Ma bedrock dates in the Donjek watershed are not among the Donjek detrital dates.

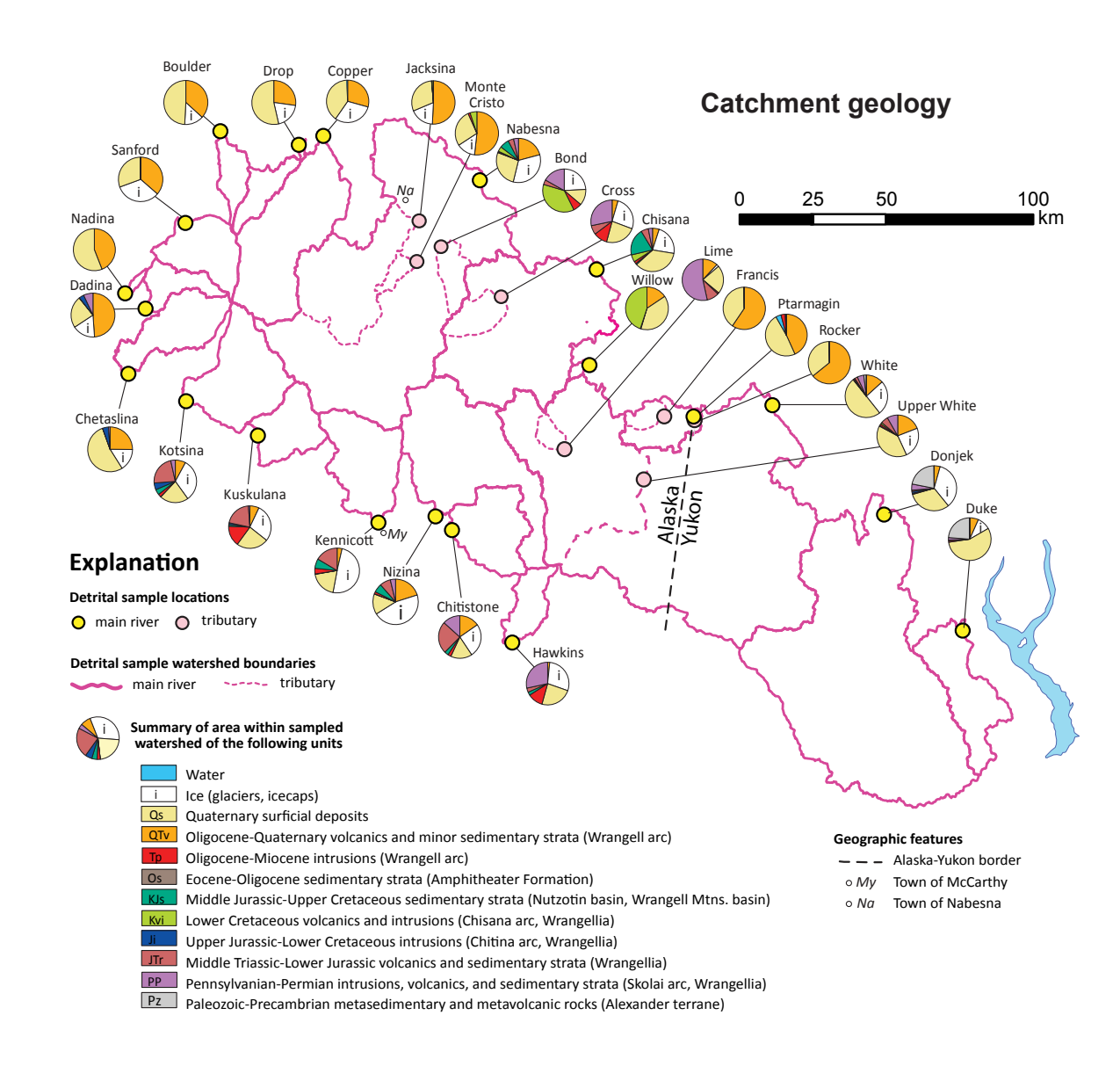


Figure 4. Summary of ice, surficial deposits, and bedrock units within the sampled watersheds is provided. Refer to Figures 2 and Item S5 (text footnote 1) for additional geologic context.

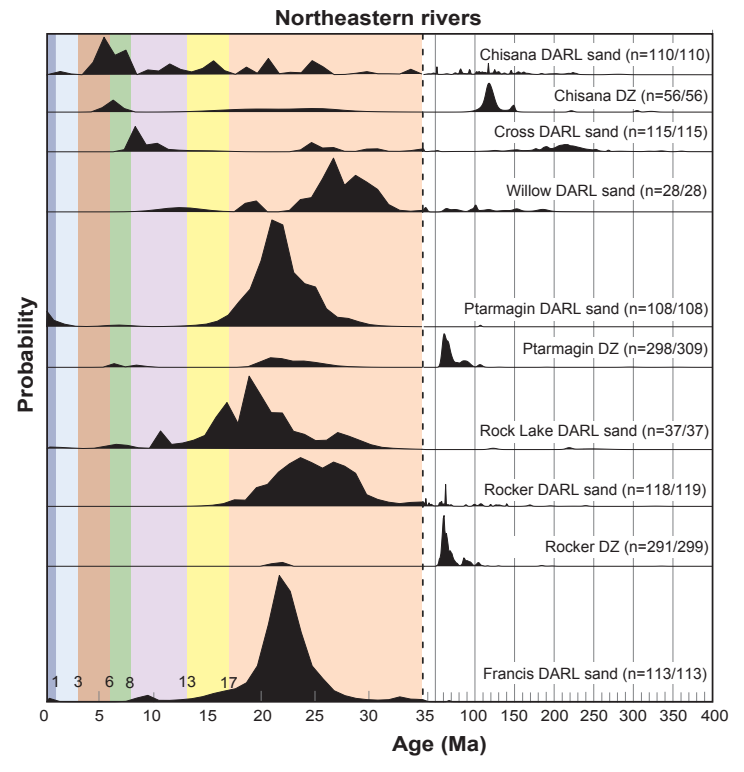


Figure 5. Normalized distribution plots of detrital samples from modern rivers in the draining northeastern flank of the Wrangell–St. Elias Mountains are shown. Bottom plots show <400 Ma dates; top plots show details of <35 Ma dates. DARL—volcanic rock lithic, DZ—detrital zircon.

Southern Rivers

Sediment samples from six modern rivers that drain the south flank of the Wrangell Mountains yield chiefly Cenozoic (63%) and subordinate Mesozoic (28%), Paleozoic (10%), and Precambrian (<1%) detrital dates (n = 1763) (Figs. 7, 10, and Items S9–S12 [footnote1]). Ages >35 Ma represent 40% of the population and consist of three main populations between 57 Ma and 51 Ma (Paleogene), 174 Ma and 137 Ma (Jurassic–Cretaceous), and 320 Ma to 288 Ma (Pennsylvanian–Permian). The proportion of >35 Ma dates is comparable among DZ (39%) and DARL (43%) sand fractions. Ages of <35 Ma represent 60% of the detrital population in sediment sampled from southern rivers, including 61% of DZ dates, 57% of sand-sized DARL dates, and 90% of cobble-sized DARL dates. Ages between 12 Ma and 3 Ma are most common within the <35 Ma detrital population. Detrital dates generally young

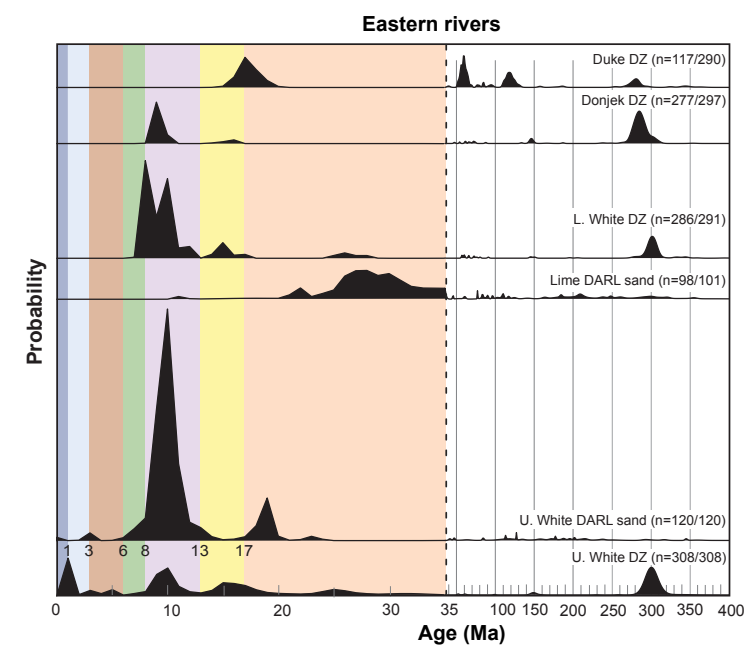


Figure 6. Normalized distribution plots of detrital samples from modern rivers in the draining eastern flank of the Wrangell–St. Elias Mountains are shown. Bottom plots show <400 Ma dates; top plots show details of <35 Ma dates. DARL—volcanic rock lithic, DZ—detrital zircon.

northwestward among the rivers sampled. Samples from the Hawkins, Chitistone, and Nizina Rivers yield dominant DZ populations between 3 Ma and 6 Ma, 8 Ma and 13 Ma, and 6 Ma and 8 Ma, respectively. To the northwest, the Kennicott, Kotsina, and Kuskulana Rivers show dominant DZ populations between 3 Ma and 6 Ma. DARL dates show a broadly similar trend. In the southeast, samples from the Hawkins, Chitistone, and Nizina Rivers reveal DARL dates that are dominantly 3–6 Ma, 8–13 Ma, and 8–13 Ma, respectively. In the northwest, the Kennicott, Kotsina, and Kuskulana Rivers yield DARL dates that are dominantly <1 Ma, 3–6 Ma, and <1 Ma, respectively.

Southern river detrital dates overlap with 3–13 Ma bedrock dates reported from southern watersheds. However, detrital samples yield a much broader distribution of dates than bedrock data reported from southern watersheds. DZ dates between 1 Ma and 3 Ma and 3 Ma to 6 Ma in the Kennicott River, and 6–8 Ma DZ dates in the Nizina and Chitistone Rivers, lack matching bedrock dates in their watersheds. Moreover, DARL dates between 1 Ma and 3 Ma in the Kotsina River; 1–3 Ma, 3–6 Ma, and >8 Ma in the Kennicott River; 6–8 Ma in the Nizina River; and 17–35 Ma in the Chitistone River lack corresponding bedrock dates within their watersheds.

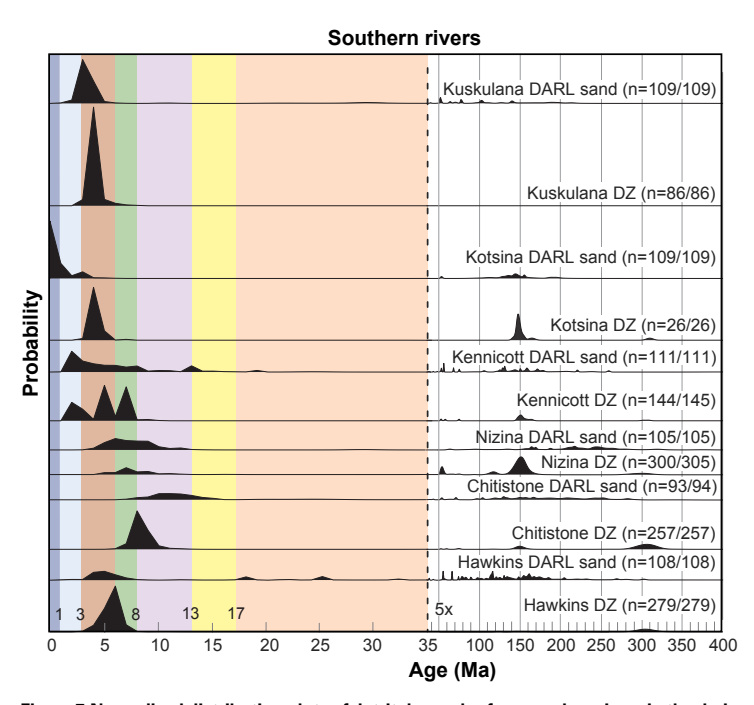


Figure 7. Normalized distribution plots of detrital samples from modern rivers in the draining southern flank of Wrangell–St. Elias Mountains. Bottom plots show <400 Ma dates; top plots show details of <35 Ma dates. Note that the detrital zircon age spectra >50 Ma is vertically exaggerated 5x. DARL—volcanic rock lithic, DZ—detrital zircon.

Northwestern rivers Copper DARL sand (n=101/101) Copper DZ (n=77/77) Drop DARL sand (n=110/110) Drop DZ (n=251/251 Boulder DARL sand (n=48/48) Boulder DZ (n=120/122) Probability Sanford DARL sand (n=117/117 Sanford DZ (n=158/158) Nadina DZ (n=83/83) Dadina DARL sand (n=114/114) Dadina DZ (n=83/83) Chetaslina DARL sand (n=221/221) Chetaslina DZ (n=110/110) 13 35 10 15 20 25 30 100 150 200 250 300 350 400 Age (Ma)

Figure 8. Normalized distribution plots of detrital samples from modern rivers in the draining northwestern flank of the Wrangell–St. Elias Mountains are shown. Bottom plots show <400 Ma dates; top plots show details of <35 Ma dates. Note that the detrital zircon age spectra >50 Ma is vertically exaggerated 5x. DARL—volcanic rock lithic, DZ—detrital zircon.

Northwestern Rivers

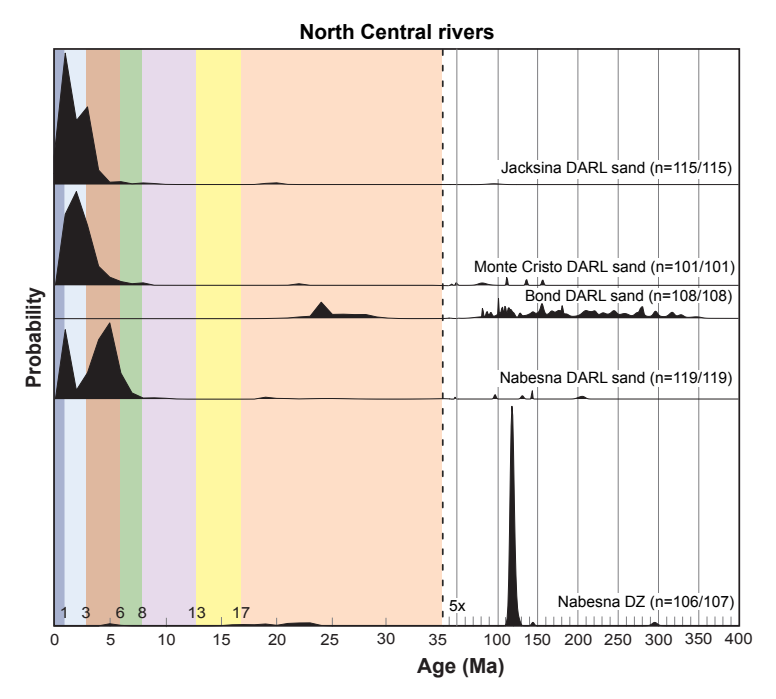
Sediments from seven modern rivers traversing the northwestern Wrangell Mountains reveal Cenozoic (73%), Mesozoic (24%), and Paleozoic (3%) detrital dates (n = 1642) (Figs. 8, 10, and Items S9–S12 [footnote 1]). Dates >35 Ma represent 28% of the detrital population and include three main populations between 136 Ma and 120 Ma (Cretaceous), 152 Ma and 141 Ma (Jurassic–Cretaceous), and 313 Ma and 289 Ma (Pennsylvanian–Permian). Dates >35 Ma are more common in the DZ sand fraction (50%) than in the DARL sand fraction (1%). Dates of <35 Ma represent 72% of the population in northwestern river samples, including ~50% of DZ dates, 99% of sand-sized DARL dates, and ~96% of cobble-sized DARL dates. DZ dates of <3 Ma dominate, making up ~41% of DZ dates and ~81% of DARL dates. Samples from the Nadina, Sanford, Boulder, Drop, and Copper Rivers yield dominant <1 Ma populations along with subordinate 1–3 Ma populations for both DZ and DARL. The Dadina River shows dominant populations of <1 Ma and 1–3 Ma for DARL and DZ,

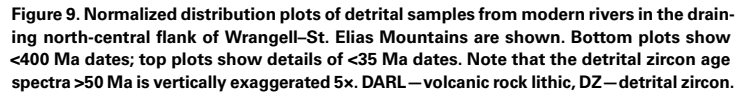
respectively. The Chetaslina River exhibits a dominant population of <1 Ma DARL dates and no <35 Ma DZ dates.

Northwestern rivers yield chiefly <3 Ma dates that correspond with dominantly <3 Ma bedrock dates among northwestern watersheds. However, several rivers show subordinate 1–3 Ma dates in watersheds that lack 1–3 Ma bedrock dates. Moreover, minor populations of >3 Ma DZ and DARL dates are absent in the available bedrock data.

North-Central Rivers

Sediment samples from seven modern rivers traversing the north-central Wrangell Mountains show Cenozoic (62%), Mesozoic (32%), Paleozoic (5%), and Precambrian (1%) detrital dates (n = 561) (Figs. 9, 10, and Items S9–S12 [footnote 1]). Dates >35 Ma represent 38% of the population and include a major population between 123 Ma and 115 Ma (Early Cretaceous), as well as sparse





dates between 340 Ma and 130 Ma (Early Cretaceous–Mississippian). Ages >35 Ma are substantially more common in the DZ sand fraction (94%) than in the DARL sand fraction (25%). Ages of <35 Ma dominate north-central rivers overall (62% of all detrital dates) but the proportion of <35 Ma ages varies from 6% of DZ dates to 75% of sand-sized DARL dates and ~83% of cobble-sized DARL dates. The Nabesna River watershed exhibits substantial variations in detrital dates. Sparse DZ dates from the Nabesna River are chiefly >17–35 Ma along with subordinate 11–13 Ma and 3–6 Ma dates. DARL dates from the Nabesna River include a dominant population between 3 Ma and 6 Ma and minor populations of <3 Ma, 6–8 Ma, and 17–35 Ma. Nabesna River tributaries exhibit these variations; the Jacksina, Monte Cristo, and Bond tributaries show dominant DARL dates of <1 Ma, 1–3 Ma, and 17–35 Ma, respectively.

Detrital dates obtained from north-central river sediment samples generally overlap with bedrock dates reported from watersheds. However, mismatches occur locally. Specifically, Nabesna River DZ samples lack <3 Ma and 6–8 Ma dates, which are evident in bedrock data, and the Jacksina tributary yields 3–6 Ma DARL dates that are not captured in the available bedrock age data.

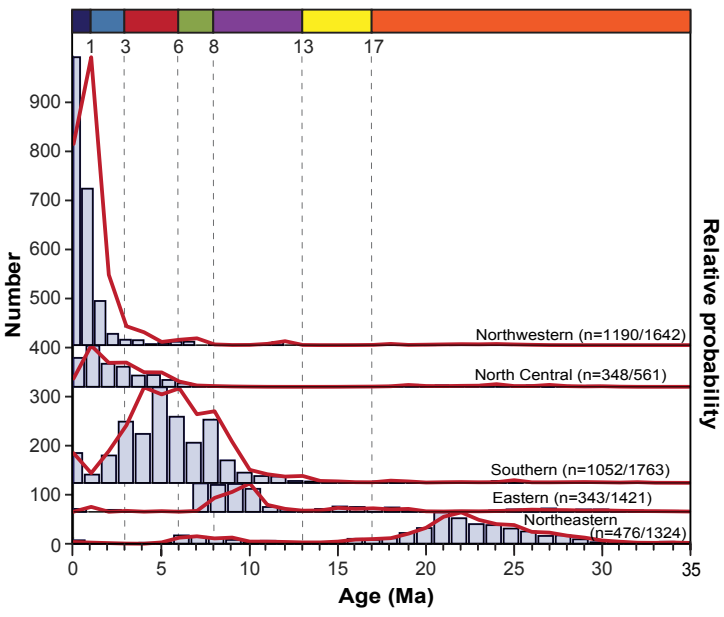


Figure 10. Probability density plots summarize <35 Ma detrital dates from modern rivers that drain the Wrangell–St. Elias Mountains. Plots include all detrital zircon (DZ) U-Pb dates as well as sand- and cobble-sized volcanic lithic (DARL) 40Ar/39Ar dates.

DISCUSSION

Provenance

DZ and DARL dates from modern river sediments in the watersheds sampled reflect derivation chiefly from primary volcanic and plutonic sources with smaller contributions from secondary sedimentary and metasedimentary sources. Sparse populations of early Paleozoic (440 Ma apparent age peak) and Precambrian detrital dates (1710–2110 Ma, 2460–2840 Ma) recovered chiefly from eastern rivers are comparable to bedrock age populations reported from the Alexander and Yukon-Tanana terranes within the sampled watersheds as well as outside the watersheds in eastern Alaska, Yukon Territory, and southeastern Alaska (Pz in Figs. 2, 4, and Item S5). Alexander terrane Paleozoic–Proterozoic rocks show dominant apparent age peaks between 490 Ma and 410 Ma and 610 Ma and 520 Ma, and minor peaks span 2300–900 Ma (Beranek et al., 2014; Tochilin et al., 2014; White et al., 2016). Yukon-Tanana terrane Paleozoic metasedimentary strata yield 2000–1700 Ma apparent age

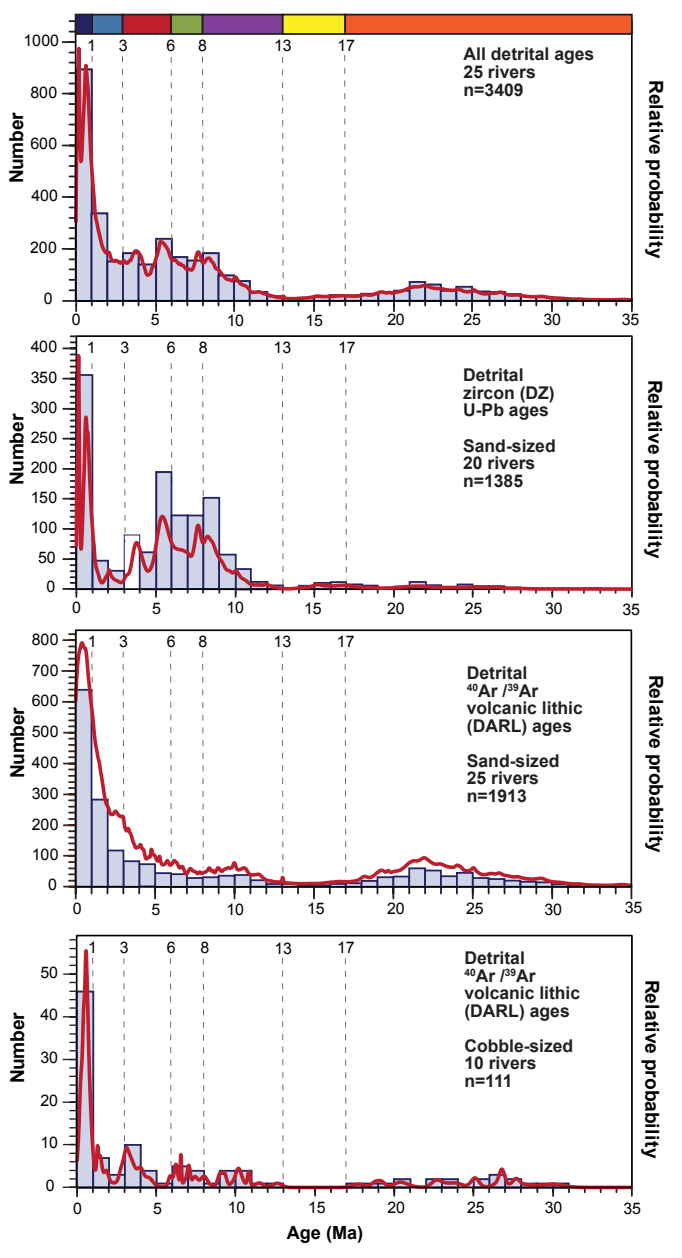


Figure 11. Probability density plots of <35 Ma detrital dates from modern rivers are shown. (A) All detrital dates, (B) detrital zircon (DZ) U-Pb dates, (C) sand-sized volcanic rock lithic 40Ar/39Ar (DARL) dates, and (D) cobble-sized volcanic rock lithic 40Ar/39Ar DARL dates.

peaks and 380–340 Ma intrusive suites (Aleinikoff et al., 1981, 1984, 1986; Dusel-Bacon et al., 2006; Nelson and Gehrels, 2007; Dusel-Bacon and Williams, 2009; Day et al., 2014; Pecha et al., 2016).

Subordinate 320–270 Ma detrital dates (301 Ma apparent age peak) from the sampled rivers correspond with late Paleozoic magmatism in the Insular terranes (Skolai Arc in Fig. 12). In the watersheds sampled and adjacent parts of eastern Alaska and Yukon, the late Paleozoic magmatic suite consists of ca. 360–273 Ma volcanic and volcaniclastic rocks, intrusions, and sedimentary strata (PP in Figs. 2, 4, and Item S5 [footnote 1]; Smith and MacKevett, 1970; MacKevett, 1971; Read and Monger, 1976; Beranek et al., 2014) that record island arc magmatism, slab breakoff, and post-collision arc magmatism (Greene et al., 2009; Beranek et al., 2014; Israel et al., 2014).

Sparse 270–220 Ma detrital dates record erosion of 233–222 Ma plume-related volcanics, intrusions, and associated sedimentary rocks (JTr in Figs. 2, 4, and Item S5 [footnote 1]; Wrangellia flood basalt in Fig. 12) that formed within the remnant late Paleozoic island arc (Mortensen and Hulbert, 1992; Greene et al., 2010). The paucity of both DZ and DARL dates matching the emplacement age of this igneous suite is consistent with the low zircon fertility that typifies basaltic igneous rocks, evidence for thermal resetting of the argon thermochronologic system within the Triassic igneous rocks (Greene et al., 2010), and our DARL sampling strategy that targeted fresh, unaltered volcanic lithics.

A minor population of 160–140 Ma (apparent age peak of 145 Ma) DZ and DARL dates reflects erosion of Late Jurassic–Early Cretaceous magmatic arc igneous rocks and associated sedimentary strata (Chitina arc in Fig 12; Ji and KJs in Figs. 2, 4, and Item S5 [footnote 1]). In the sampled watersheds and adjacent parts of eastern Alaska, Chitina Arc plutons yield 150–138 Ma dates (Plafker et al., 1989; Roeske et al., 2003). Late Jurassic detrital dates also reflect erosion of Mesozoic sedimentary and volcanic rocks that crop out within the sampled watersheds (JTr and JKs in Figs. 2, 4, and Item S5 [footnote 1]) and yield abundant 160–140 Ma detrital zircon dates (Fasulo et al., 2020) and 191–145 Ma 40 Ar/33 Ar dates (Greene et al., 2010). Chitina Arc magmatism overlapped with subduction, arc magmatism, and deformation across the Insular terranes between 160 Ma and 140 Ma in the Yukon, British Columbia, and southeastern Alaska (van der Heyden, 1992; Gehrels et al., 2009; Berenek et al., 2017) and between 180 Ma and 140 Ma in south-central Alaska (Rioux et al., 2007; Finzel and Ridgway, 2017; Stevens Goddard et al., 2018).

A subordinate population of 130–110 Ma (apparent age peak of 117 Ma) DZ and DARL dates corresponds with erosion of late Early Cretaceous arc igneous rocks and associated sedimentary strata (Chisana Arc in Fig. 12; Kvi and KJs in Figs. 2, 4, and Item S5 [footnote 1]). The largest 130–110 Ma apparent age peaks are in samples from north-central and northeastern rivers draining watersheds with aerially extensive Chisana Arc igneous rocks (e.g., Chisana, Cross, and Nabesna Rivers in Figs. 3, 4, and Item S5 [footnote 1]). In the watersheds sampled and adjacent parts of eastern Alaska, the Chisana Arc yields ages of 126–113 Ma, judging from 40 Ar/ 40 Ar and U-Pb dates (Snyder and Hart, 2007; Graham et al., 2016; Trop et al., 2020; Manselle et al., 2020). Dates of 130–110 Ma from the watersheds sampled reflect erosion of arc igneous rocks

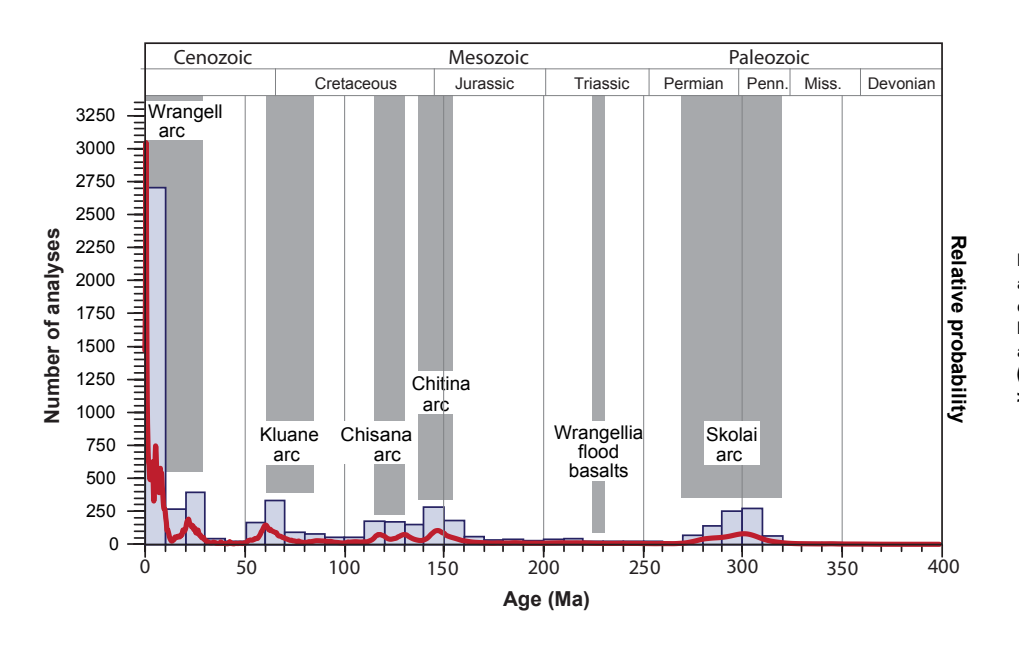


Figure 12. Probability density plots summarize all <400 Ma detrital dates from 25 modern rivers that drain the Wrangell–St. Elias Mountains. Plots include all detrital zircon (DZ) U-Pb dates and sand- and cobble-sized volcanic rock lithic (DARL) ⁴⁰Ar/³⁹Ar dates. Not shown are sparse >400 Ma dates (3% of total population).

as well as recycling of late Early to Late Cretaceous sedimentary strata that bear apparent age peaks of 130–110 Ma (Fasulo et al., 2020; Trop et al., 2020). Correlative igneous and sedimentary strata crop out regionally to the east in southeastern Alaska and Canada (Gehrels, 2000; Yokelson et al., 2015) and to the northwest in the Talkeetna Mountains and the Alaska Range (Hampton et al., 2010; Reid et al., 2018; Stevens Goddard et al., 2018; Trop et al., 2019; Box et al., 2019). Subordinate 70–55 Ma (apparent age peak of 62 Ma) DZ dates correspond with erosion of latest Cretaceous–Paleocene arc igneous rocks that are uncommon within the sampled watersheds but crop out regionally in the Alaska Range and the Yukon (Kluane Arc of Plafker and Berg, 1994).

The <35 Ma dominant population of DZ and DARL dates reflects erosion of Oligocene–Quaternary Wrangell Arc volcanic-intrusive rocks, which constitute ~16% of the surface area of watersheds sampled (Figs. 2–4 and Item S5 [footnote 1]). Notably, Wrangell Arc volcanic-intrusive rocks likely underlie extensive portions of ice that make up 29% of the watersheds sampled (Item S5), judging from Wrangell Arc bedrock exposures protruding above ice (Figs. 2–3) and the dominance of <35 Ma DARL dates in modern rivers located downslope of glacial ice. Below, the Discussion summarizes the spatial-temporal evolution of the Wrangell Arc as inferred from the available geochronologic data.

In summary, modern river detrital and bedrock dates obtained during the present study, with previously reported bedrock dates, document erosion of magmatic arcs with the following apparent age peaks: 301 Ma, 145 Ma, 132 Ma, 116 Ma, 62 Ma, and <35 Ma (Fig. 12). Sparse detrital dates also record a single

phase of Triassic plume magmatism that is associated with mafic large igneous province development.

Implications for Sediment Provenance Analysis

Assessment of DZ and DARL dates from modern river sediment in the Wrangell Arc adds to the growing number of studies demonstrating the additional insight afforded by multi-proxy detrital geochronology (e.g., Nie et al., 2012; Bush et al., 2016; Di Giulio et al., 2017; Arboit et al., 2020). DZ populations reveal higher proportions of Mesozoic-Paleozoic arc igneous sources that are missing or incomplete in DARL populations, whereas DARL populations record higher proportions of Neogene arc igneous sources that are missing or incomplete in DZ age spectra (refer to Item S13 for details [footnote 1]). Higher zircon fertility from plutons with ages >35 Ma and recycling from sedimentary deposits contribute a disproportionate and greater volume of detrital zircon grains relative to generally mafic <35 Ma volcanic sources. This interpretation is compatible with higher average zircon concentrations reported from the majority of >35 Ma igneous rocks in the study region compared with <35 Ma Wrangell Arc igneous rocks (Berkelhammer et al., 2019; Brueseke et al., 2019; Manselle et al., 2020), and we acknowledge that geochemical data from >35 Ma rocks are not abundant. Although not unexpected, this relationship underscores the potential for disproportionate detrital zircon contributions eroded from older, mainly felsic arc plutons or recycled from sediments.

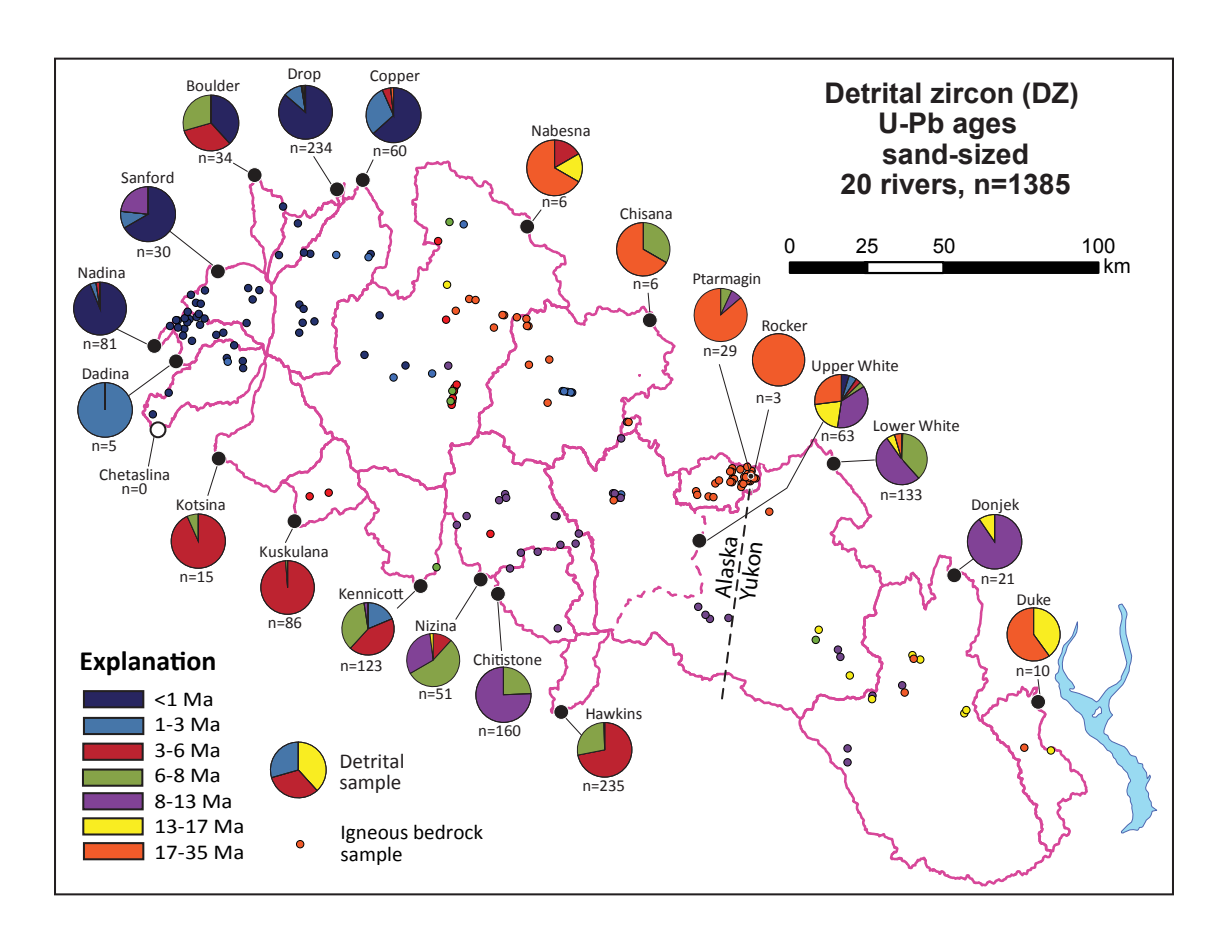


Figure 13. Map summarizes <35 Ma detrital zircon (DZ) U-Pb dates (pie diagrams), watershed boundaries (pink lines), tributary watershed boundaries (dashed pink lines), and bedrock ages.

Arc Episodicity and Flare-Ups

Assessment of geochronological records from the Wrangell Arc in eastern Alaska adds to the growing evidence for non-steady-state behavior in arc magmatism along the eastern Pacific margin. Wrangell Arc geochronologic data indicate episodes of high-volume arc magmatism alternating with periods of reduced magmatism during Paleozoic-Holocene time (Fig. 12), which is comparable to the high-volume arc magmatism with apparent cyclicity of ~15-35 m.y. documented in other Alaskan arc segments in the Aleutian Islands (Jicha et al., 2006), Alaska Peninsula (Finzel and Ridgway, 2017), Alaska Range (Fasulo, 2019; Jones et al., 2021), and Talkeetna Mountains (Reid et al., 2018; Stevens Goddard et al., 2018). Further south, high-volume arc magmatism with apparent cyclicity of ~25 m.y. to >50 m.y. is evident along the Cordilleran margin from western Canada to South America (Ferrari et al., 1999; Haschke et al., 2006; Trumbull et al., 2006; Gehrels et al., 2009; Girardi et al., 2012;

Paterson et al., 2014; Premo et al., 2014; DeCelles et al., 2015; Beranek et al., 2017). Models explaining arc episodicity invoke plate motion controls (Jicha et al., 2018), intra-arc processes (Ducea and Barton, 2007; DeCelles et al., 2009), or crustal modulation of mantle power input (de Silva et al., 2015).

Wrangell Arc geochronologic data and offshore Gulf of Alaska tephra records (Benowitz and Addison, 2017) indicate an apparent increase in magmatic flux at ca. 1 Ma, although the trend may be impacted by decreased marine core recovery with depth-time, sample biases, the better preservation of younger volcanic rock products, and the younger eruptive centers covering older volcanic centers. A ca. 1 Ma flare-up would be coeval with increased amplitude glacial-interglacial variability documented during the mid-Pleistocene transition (1.25-0.7 Ma; Willeit et al., 2019) across the Northern Hemisphere and southern Alaska (Gulick et al., 2015). Volcanic activity increased worldwide during this time period as a result of glacial-interglacial cycles ("glacial pumping"; Wilson and Russell, 2020).

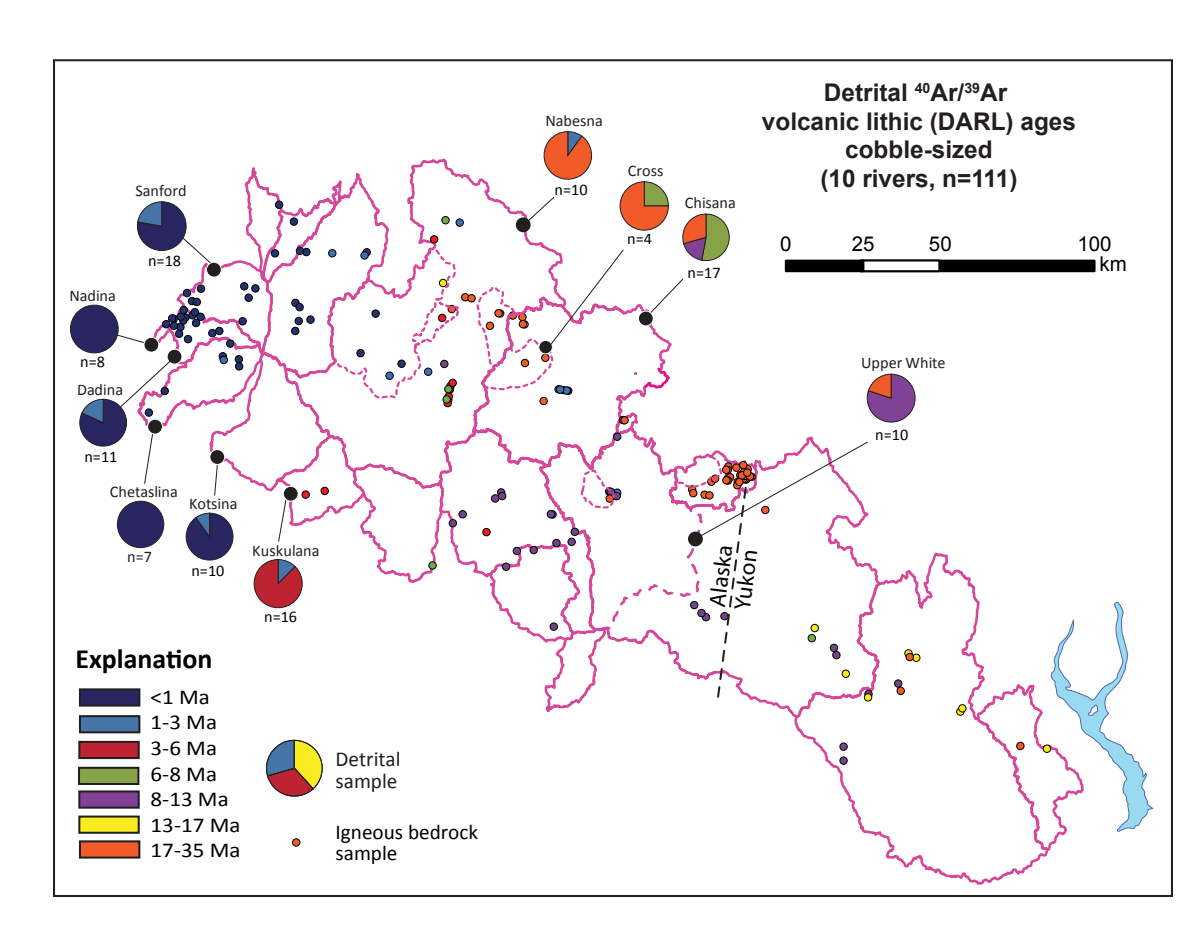


Figure 14. Map summarizing <35 Ma detrital sand-sized volcanic rock lithic (DARL) ⁴⁰Ar/³⁸Ar dates (pie diagrams), watershed boundaries (pink lines), tributary watershed boundaries (dashed pink lines), and bedrock dates.

Strike-Slip Deformation along Intra-Arc Faults

Geologic observations indicate that dextral-oblique slip occurred along the Denali and Totschunda faults (Figs. 1–3) throughout 30 Ma to Holocene Wrangell Arc magmatism. Offset features along the Denali and Totschunda faults indicate dextral-oblique slip during Paleocene–Holocene time (Haeussler et al., 2017). Metamorphic complexes exposed adjacent to the easterly Denali fault reflect dextral transpressional exhumation at ca. 20–6 Ma (Richter et al., 1975; Benowitz et al., 2011, 2012b, 2014, 2019; Tait et al., 2016). Estimated Cenozoic displacements along the strike-slip easterly Denali fault system are ~400 km (Denali and Totschunda fault combined) since 57 Ma (Lowey, 1998; Riccio et al., 2014) and ~305 km since 33 Ma (Waldien et al., 2018b). Along the western Denali fault, where a larger component of thrusting accommodates fault displacement (Fitzgerald et al., 2014), offset markers indicate ~150 km of dextral slip since 29 Ma (Trop et al., 2019). Collectively, the available

observations indicate the eastern Denali fault accommodated ~180 km of dextral slip between ca. 30 Ma and 6 Ma at a time-averaged rate of ~7.6 mm/ yr with minimum and unknown slip after ca. 6 Ma.

The Totschunda fault was active during Wrangell Arc magmatism, considering evidence for diking within the fault zone at ca. 29 Ma (Brueseke et al., 2019), rapid exhumation along the fault at ca. 25 Ma (Milde et al. 2013), and transtensional basin development between 13 Ma and 10 Ma (Trop et al., 2012). Offset geologic piercing points along the Totschunda fault indicate ~90 km of dextral slip since 7 Ma (Waldien et al., 2018b), as much as ~85 km of dextral slip since ca. 18 Ma (Berkelhammer et al., 2019), and a Pleistocene rate of 14 mm/yr (Marechal et al., 2018). The available geologic data indicate the following dextral slip estimates along the Totschunda fault: ~14 mm/yr offset totaling 85 km from 6 Ma to present and 0.6 mm/yr totaling ~15 km between 30 Ma and 6 Ma. In the following section, we combine these offset estimates with geochronologic data from the Wrangell Arc to reconstruct the spatial-temporal evolution of Wrangell magmatism.

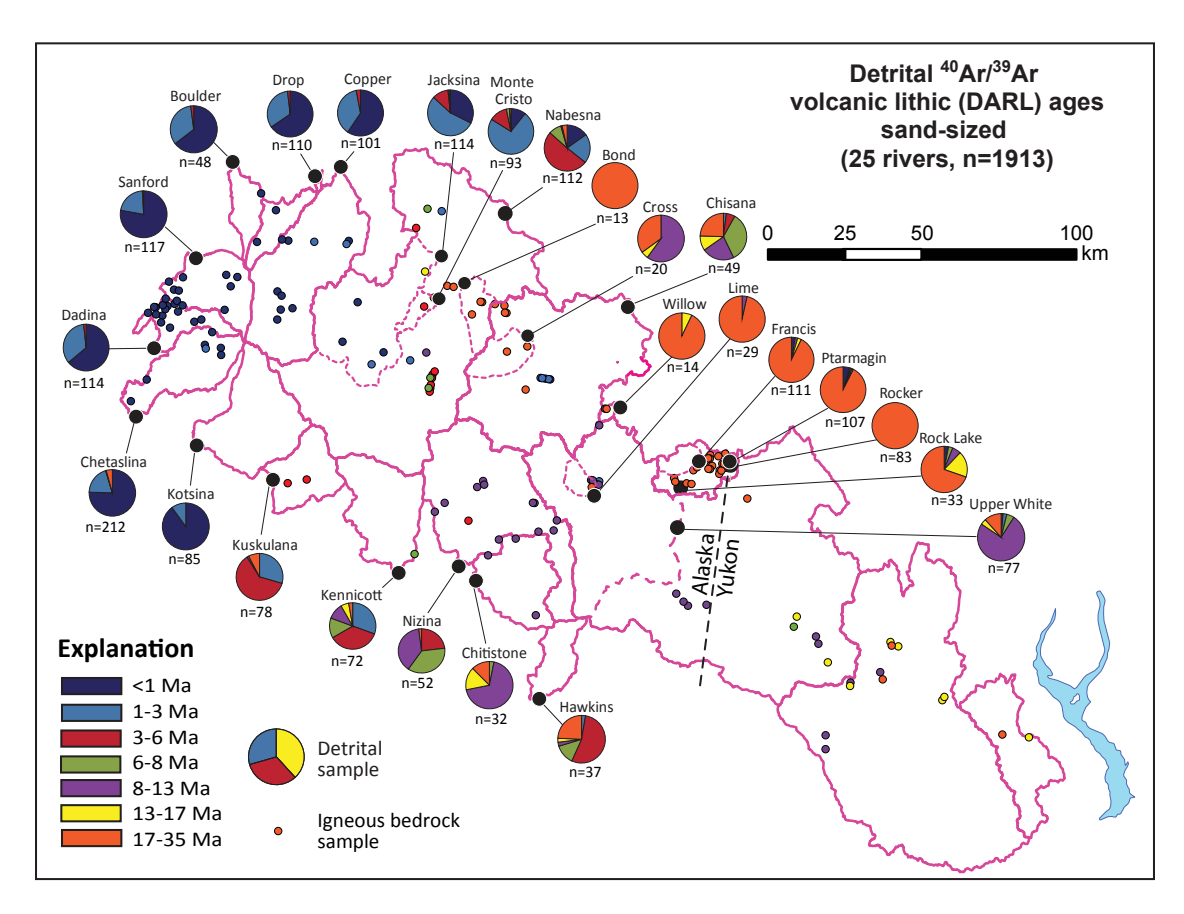


Figure 15. Map summarizes <35 Ma detrital cobble-sized volcanic rock lithic ⁴⁰Ar/³⁹Ar (DARL) dates (pie diagrams), watershed boundaries (pink lines), tributary watershed boundaries (dashed pink lines), and bedrock dates.

Spatial-Temporal Evolution of Wrangell Magmatism

Wrangell Arc magmatism initiated along the northern flank of the Wrangell–St. Elias Range at ca. 30 Ma, based on currently available geochronologic data (Berkelhammer et al., 2019; Brueseke et al., 2019; this study). The oldest known Wrangell Arc eruptive centers crop out on both sides of the Totschunda fault within the north-central and northeastern river watersheds (Figs. 16–17). North of the fault, 30–19 Ma magmatism prompted construction of the Sonya Creek volcanic field (SCVF in Figs. 1, 16, and 17), judging from new DZ and DARL dates from Ptarmigan, Rocker, Francis, and Rock Lake and recently reported volcanic/intrusive bedrock dates (Berkelhammer et al., 2019). The Upper White and Lower White Rivers also yield minor populations of 30–17 Ma DZ and DARL dates that may reflect sediment contributions from tributaries that extend into the SCVF. However, much of the White and Lower White drainages traverse bedrock southwest of SCVF. At ca. 30–17 Ma, eruptive centers also formed along the west

side of the Totschunda fault; north-central watersheds yield 30–17 Ma DZ and DARL dates (Bond, Chisana, and Cross tributaries) and several K-Ar intrusive bedrock dates. Ca. 30–17 Ma eruptive centers exposed on opposite sides of the Totschunda fault were likely proximal to one another and subsequently offset by dextral displacement along the Totschunda fault (B and SCVF in Figs. 16–17).

Wrangell magmatism progressed from northwest to southeast ca. 18 Ma based on geochronologic data within eastern river watersheds spanning the Alaska-Yukon border (Figs. 16–17). Volcanic bedrock dates document the construction of 18–10 Ma eruptive centers presently exposed along the Duke River fault (St. Clare, Alsek, and Nines Creek fields in Figs. 1–2). The youngest population of DZ dates from the Duke (18–16 Ma) and Donjek (10–9 Ma and 16–15 Ma) watersheds overlap 18–10 Ma bedrock dates from the St. Clare field (Fig. 16), which indicates that magmatism persisted there ~1 m.y. longer than was previously recognized.

Between ca. 13 Ma and 6 Ma, Wrangell Arc magmatism generally migrated from southeast to west away from the Alaska-Yukon border region

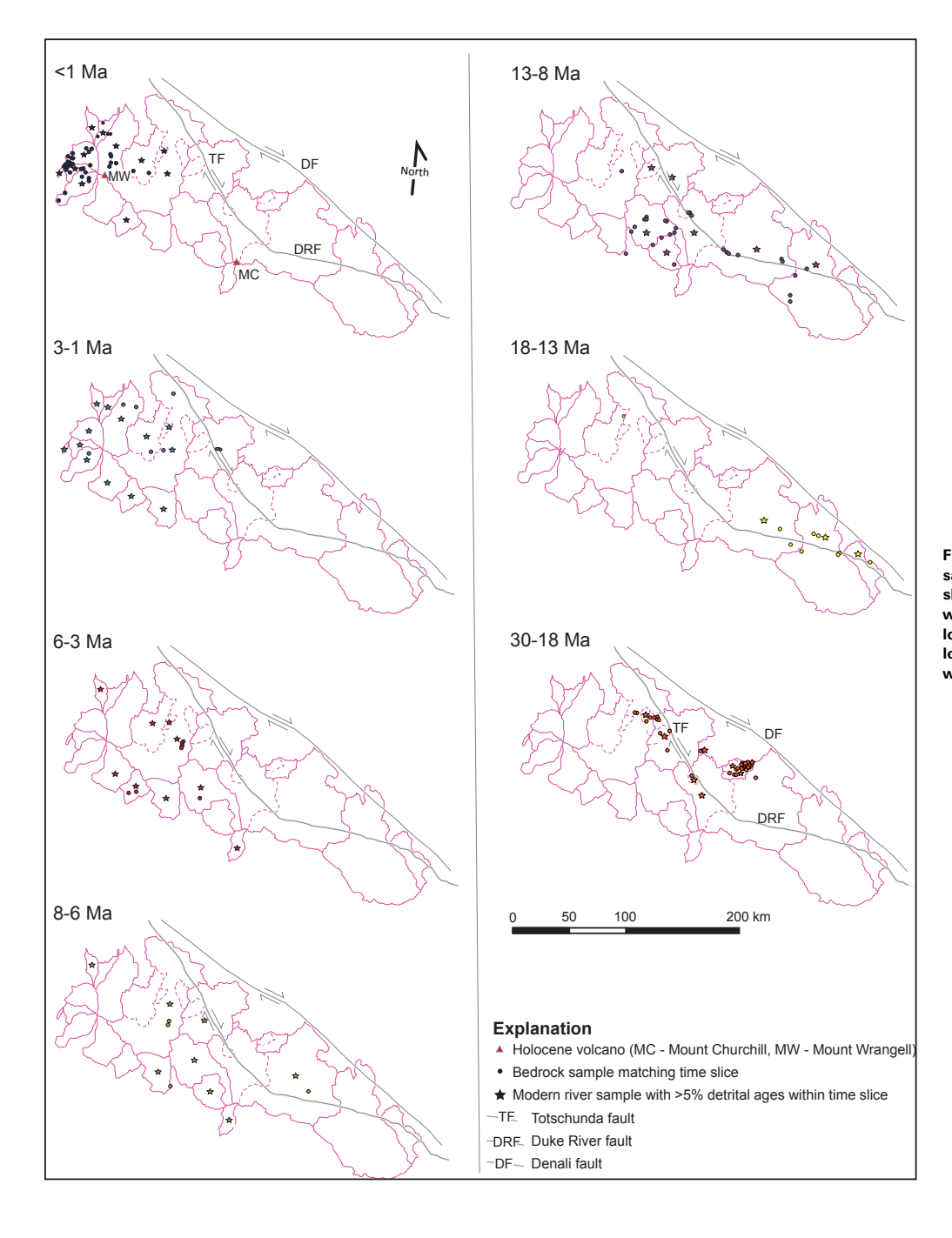


Figure 16. Maps show bedrock and detrital samples that yield dates within the time slices shown. Detrital samples are centered within watersheds to approximate sediment source locations; refer to Figure 3 for detrital sample locations. Refer to Figures 2-4 for details on watershed geology and geography.

to the Wrangell Mountains (Figs. 16-17). After ca. 6 Ma, Wrangell magmatism migrated northwestward into Holocene time (Figs. 16-17). Richter et al. (1990) demonstrated this northwestward progression using bedrock dates primarily from <3 Ma volcanics in northwestern watersheds. Trop et al. (2012) expanded the evidence with bedrock and detrital dates from 13-5 Ma volcanics in the southern watersheds. New detrital data sets in the current study add additional support for westward to northwestward progression of magmatism since 13 Ma and document previously unrecognized complexities. Some eruptive centers remained active following the progression of magmatism away from a region; moreover, some areas experienced magmatism following the general migration of magmatism away from the region. For example, magmatism persisted from 9 Ma until 2 Ma in the Kennicott watershed, following the northwestward progression of magmatism from 6 Ma until 3 Ma into the adjacent Kotsina watershed and until <3 Ma in the northwestern watersheds. Also, magmatism occurred in the Hawkins watershed from 7 Ma until 4 Ma, following the northwestward progression of magmatism away from the adjacent 12-7 Ma Chitistone and Nizina watersheds. Another exception to the apparent progression of volcanism from southeast to northwest is Mt. Churchill, a stratovolcano located tens of kilometers east of other Wrangell Arc active volcanoes (MC in Figs. 3 and 16). The volcano has produced highly explosive, volumetrically significant ash eruptions over the past 2000 years (Lerbekmo, 2008; Preece et al., 2014; Jensen et al., 2014), unlike the andesitic lavas that have erupted from most Wrangell Arc volcanoes (Richter et al., 1990). Given its location above the eastern edge of the subducting slab (Bauer et al., 2014), we posit that Mt. Churchill may be related to slab edge magmatism and that the Connector-Duke River-Totschunda fault intersection serves as a magma conduit (Fig. 2).

In summary, modern river and bedrock dates document the initiation of Wrangell Arc magmatism at ca. 30–17 Ma along both sides of the Totschunda fault, the southeastward progression of magmatism at ca. 17–10 Ma along the Duke River fault, the westward progression of magmatism outboard (southwest) of the Totschunda and Duke River faults at ca. 13–6 Ma, and a rapid northwestward progression of magmatism from ca. 6 Ma to present.

Tectonic Evolution of Wrangell Arc Magmatism

In the context of the offset history of the Denali–Duke River–Totschunda fault system, we present a model that relates long-term localization of Wrangell magmatism within and adjacent to the Cretaceous Insular terranes-North America suture zone and shifts in magmatism through time to tectonic processes (Figs. 16–19).

Arc Initiation (30-18 Ma)

Subduction-related arc magmatism initiated at ca. 30 Ma based on new detrital dates from the present study and recently reported geochronological-geochemical

data from eruptive centers exposed on both sides of the Totschunda fault along the northern flank of the Wrangell Mountains (Figs. 16-17; Berkelhammer et al., 2019; Brueseke et al., 2019). Bedrock samples from the 30-19 Ma Sonya Creek volcanic field (SCVF) indicate hydrous, subduction-related, calc-alkaline magmatism along with an adakite-like component that is attributed to slabedge melting. A minor westward progression of volcanism within the SCVF at ca. 25 Ma was accompanied by continued subduction-related magmatism without the adakite-like component (i.e., mantle-wedge melting), which is represented by 25-20 Ma basaltic-andesite to dacite domes and associated diorites and transitional-tholeiitic, basaltic-andesite to rhyolite lavas and tuffs of the 23-19 Ma Sonya Creek shield volcano (Richter et al., 2000; Berkelhammer et al., 2019). The Beaver Lake area, ~10 km west of the SCVF, is also characterized by 30-20 Ma magmatism (Fig. 3). Initial arc magmatism is also recorded along the southwestern side of the Totschunda fault west of the SCVF and Beaver Lake. Also, ca. 30-20 Ma calc-alkaline and adakitic Wrangell Arc intrusions occur proximal to the Totschunda fault in the Chisana, Cross, and Bond Creek drainages (Richter, 1976; Weber et al., 2017).

Geologic data sets indicate dextral displacement of ca. 30–20 Ma eruptive centers exposed on both sides of the presently active Totschunda fault. Dikelets that are 29.7 Ma in age and injected into Totschunda fault gouge indicate fluid flow into an active fault zone during initial arc magmatism (Brueseke et al., 2019). The fault system existed prior to Wrangell Arc magmatism, based upon 114 Ma dikelets that are injected into Totschunda fault gouge (Trop et al., 2020). Reconstructing the inferred initial alignment of the ca. 30–18 Ma eruptive centers exposed on opposite sides of the Totschunda fault requires ~85 km of dextral offset since ca. 18 Ma (Waldien et al., 2018b; Berkelhammer et al., 2019).

We attribute 30–18 Ma arc magmatism to the subduction of oceanic lithosphere along the northeastern margin of the Yakutat microplate (Figs. 1 and 17–19) during a transition in the tectonic configuration of southern Alaska between 30 Ma and 20 Ma. Regional exhumation within and proximal to the Alaska Range suture zone (Benowitz et al., 2012a; Riccio et al., 2014; Lease et al., 2016; Terhune et al., 2019; Waldien et al., 2021), basin inversion and drainage reorganization related to topographic development (Ridgway et al., 2007; Finzel et al., 2016; Brennan and Ridgway, 2015; Benowitz et al., 2019), and shortening within the Yakutat microplate (Pavlis et al., 2012, 2019) are interpreted as upper-plate responses to initial flat-slab subduction and collision of the Yakutat microplate with southern Alaska (Finzel et al., 2011; Haynie and Jadamec, 2017).

Initiation of flat-slab subduction and Wrangell Arc magmatism was coincident with the cessation of arc magmatism throughout most of the region underlain by the subducting Yakutat flat slab. Neogene arc magmatic products in the central Alaska Range are limited to a handful of small volume eruptive centers (Fig. 1; Triplehorn et al., 1999; Athey et al., 2006; Andronikov and Mukasa, 2010; Cameron et al., 2015). The 30 Ma age of the initiation of Wrangell Arc magmatism along the northeastern edge of the subducted Yakutat flat slab postdates the 33 Ma age of the youngest arc pluton in the Central Alaska Range (Regan et al., 2020), overlaps with the 29 Ma age of the youngest pluton in

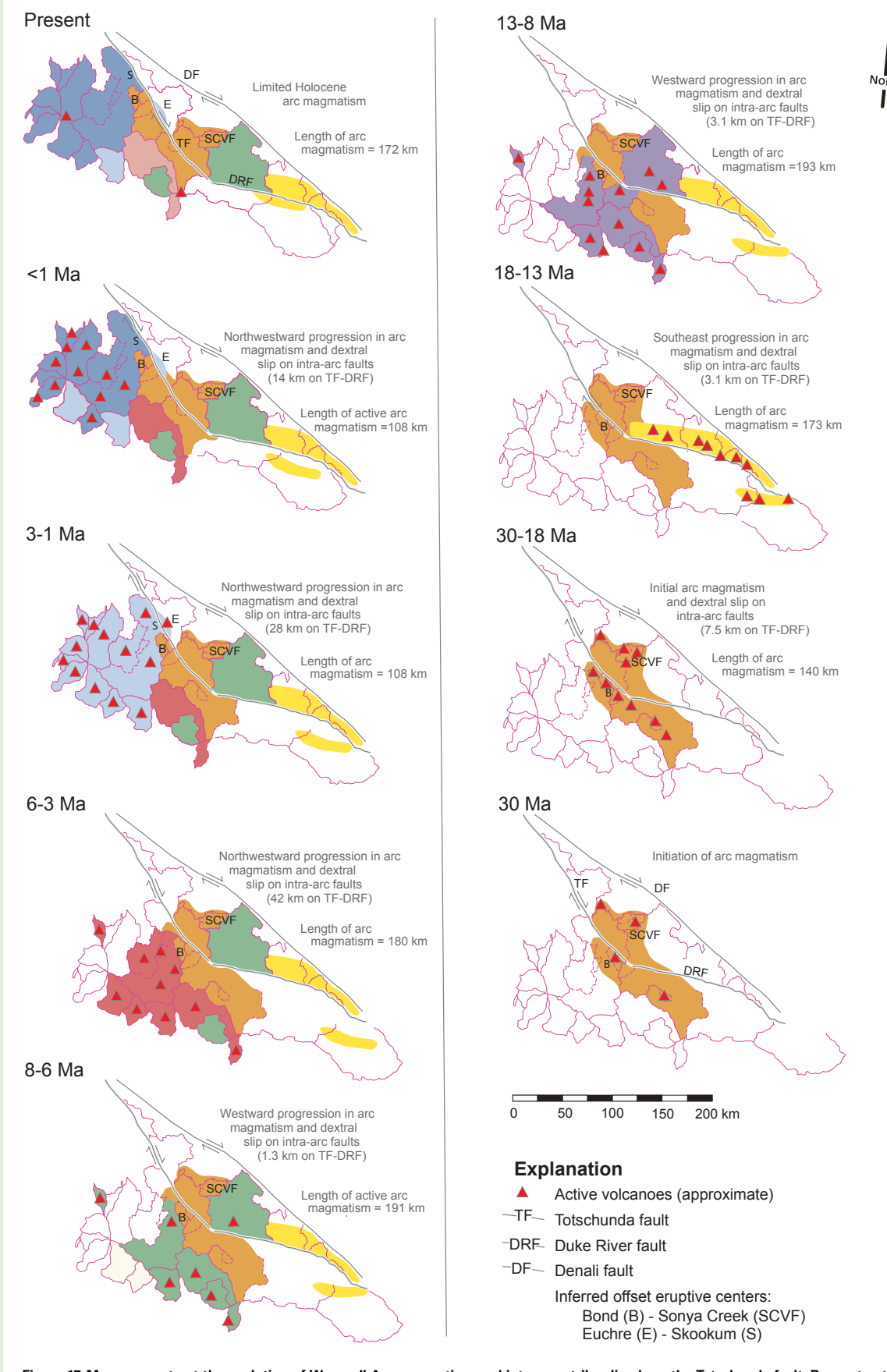
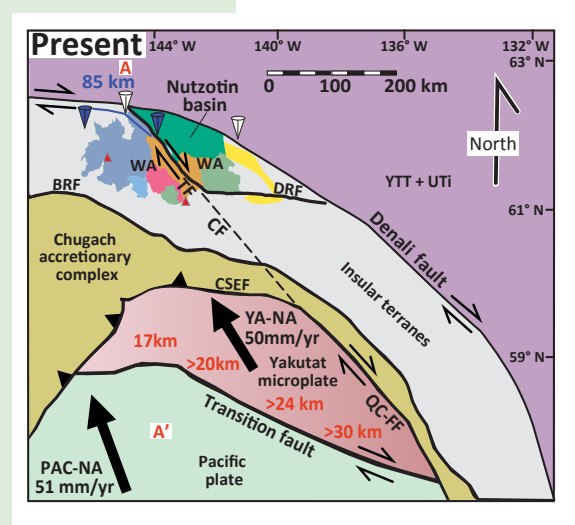
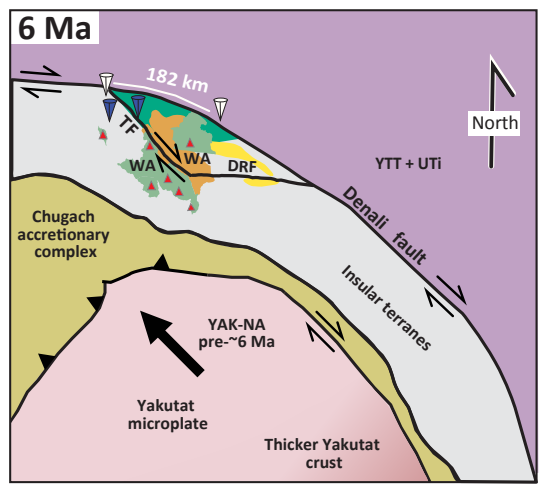
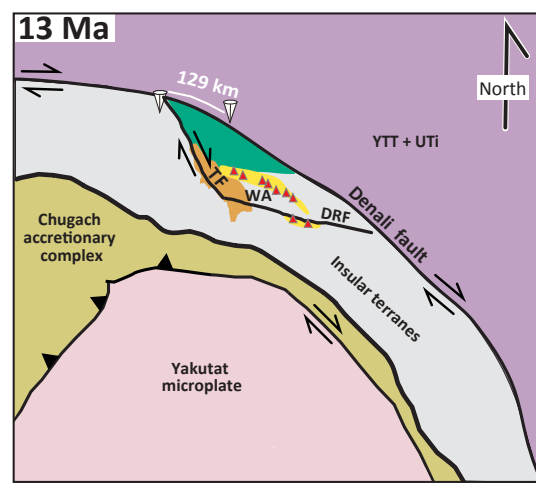
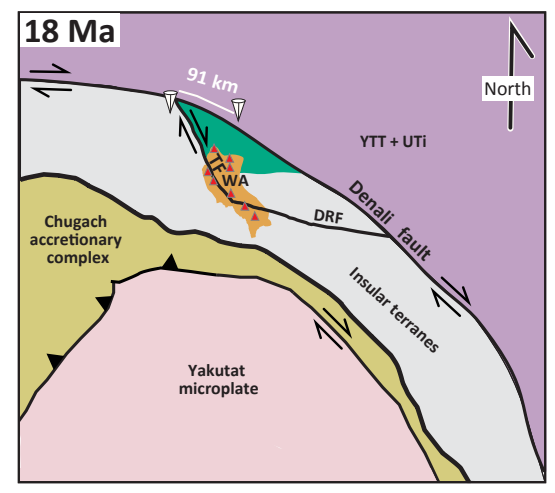


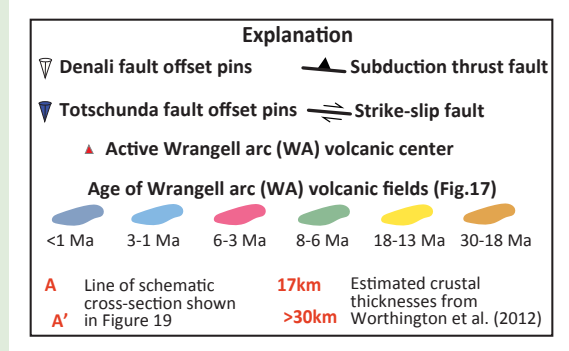
Figure 17. Maps reconstruct the evolution of Wrangell Arc magmatism and intra-arc strike-slip along the Totschunda fault. Reconstruction is based on dates summarized in Figure 15 and structural data sets summarized in Benowitz et al. (2012b), Allen et al. (2014), Allen (2016), Riccio et al. (2014), Berkelhammer et al. (2019), and Regan et al. (2021). Refer to text for discussion.











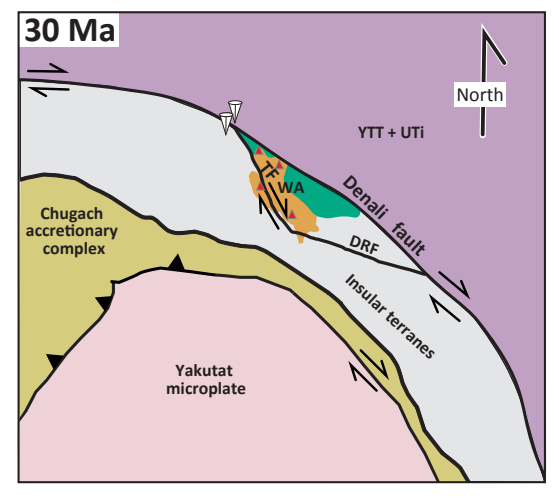


Figure 18. Schematic palinspastic reconstructions of plate interactions, magmatism, and strike-slip deformation in eastern Alaska and the Yukon from 30 Ma to present are shown. The leading northeastern edge of the Yakutat slab and Wrangell Arc magmatism track with the Totschunda-Duke River fault suture zone region from 30 Ma to 6 Ma as the Insular terranes are translated northwestward by right-lateral slip along the Denali fault. White pins demonstrate 182 km of right-

lateral slip on eastern Denali fault from 30 Ma to 6 Ma (7.6 mm/yr) (Benowitz et al., 2012b; Waldien et al., 2018b; Regan et al., 2021). Blue pins demonstrate 85 km of right-lateral slip on the Totschunda fault from 6 Ma to present (14mm/yr) (Waldien et al., 2018a, 2018b; Berkelhammer et al., 2019). Not demonstrated with pins are 15 km of allowable right-lateral slip on the Totschunda fault from 30 Ma to 6 Ma (0.6 mm/yr), but the reconstruction accounts for the additional slip on the Totschunda fault based upon the reconstruction shown in Figure 17. Slip amount on the eastern Denali fault from 6 Ma to present is not well constrained and thus is not depicted in the reconstruction, though slip likely occurred based on Holocene offset constraints (Haeussler et al., 2017). Refer to text for additional discussion of strike-slip constraints along the Denali and Totschunda faults. The Yakutat slab is pulled out based on initial subduction by 30 Ma (Brueseke et al., 2019) and insertion at modern GPS rates of 50 mm/yr (Elliot et al., 2010). Imaged outboard thickness variations (orange text) of the unsubducted Yakutat microplate are from Worthington et al. (2012). The inboard extent of the subducted Yakutat slab is shown in Figure 1. The convergence angle of subduction pre-6 Ma is shown on the 6 Ma panel (Engebretson, 1985). A-A' represents the line of cross section shown in Figure 19. Base map is modified from Waldien et al. (2018b). Abbreviations: BRF—Border Range fault system, CF—Connector fault (inferred), CSEF—Chugach-St. Elias fault, DRF—Duke River fault, QCFF—Queen-Charlotte-Fairweather fault, PAC-NA—Pacific-North America, YA-NA—Yakutat-North America, TF—Totschunda fault, UTI—undifferentiated terranes and igneous rocks, WA—Wrangell Arc, YTT—Yukon-Tanana terrane.

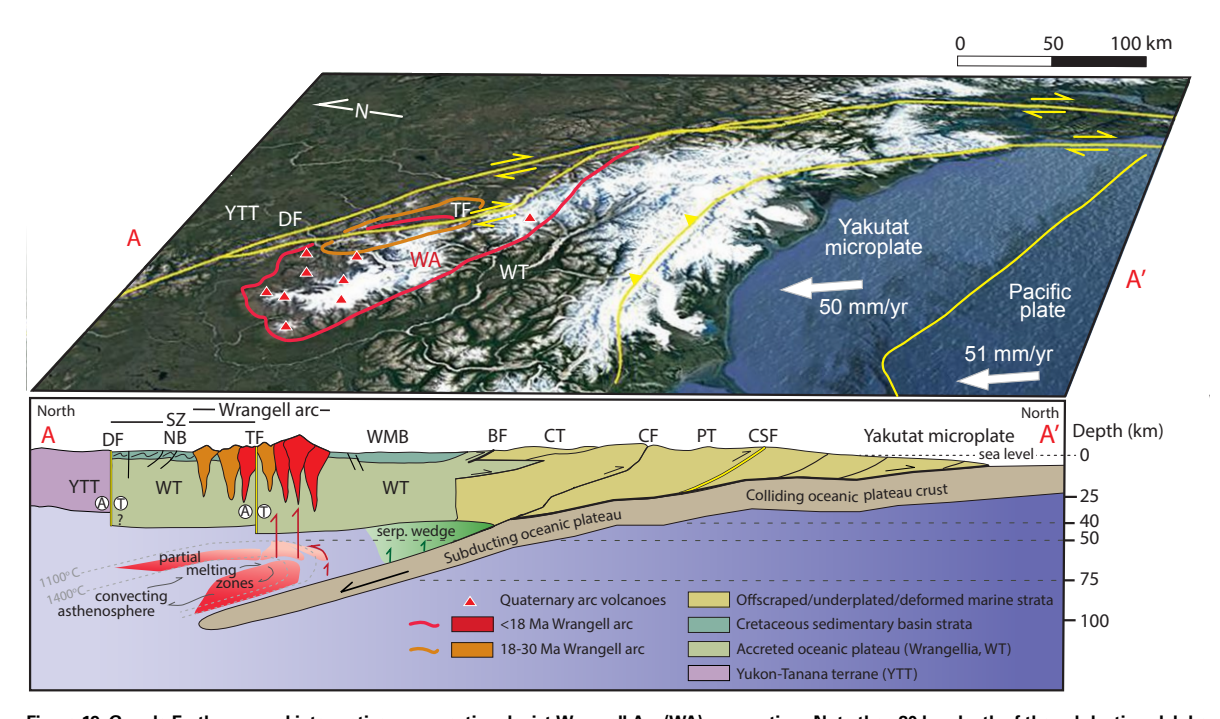


Figure 19. Google Earth map and interpretive cross-section depict Wrangell Arc (WA) magmatism. Note the ~80 km depth of the subducting slab beneath the Wrangell Arc (Pavlis et al., 2019) relative to the more typical ~100 km slab depth reported from most active magmatic arcs; this may reflect subduction of thickened oceanic crust along the leading edge of the Yakutat microplate, which is interpreted as a wedge-shaped oceanic plateau (Worthington et al., 2012). Note that Wrangell Arc magmatism has been focused within or slightly outboard of a Cretaceous suture zone (SZ) bisected by the Totschunda fault. Partial melting zones and serpentinized wedge is adapted from Leeman (2020). Crustal structure is adapted from Fuis et al. (2008), Allam et al. (2017), Pavlis et al. (2019), and Mann et al. (2020). Abbreviations: A – away, BF – Border Ranges fault, CT – Chugach terrane, DF – Denali fault, CF-Contact fault, CSF-Chugach-St. Elias fault, NB-Nutzotin basin, PT-Prince William terrane, SC-subduction components, Serp.-serpentinized, SZ-suture zone, T-toward, TF-Totschunda fault, WMB-Wrangell Mountains basin, WT-Wrangellia terrane, YTT-Yukon-Tanana terrane.

the Western Alaska Range (Jones et al., 2021), and overlaps the 38-25 Ma age range of dike swarms emplaced along the Denali fault in the Central Alaska Range (Trop et al., 2019). Thus, arc magmatism was essentially shut off in the Central and Western Alaska Range by ca. 25 Ma. This scenario is attributed to flat-slab subduction of the Yakutat microplate and changes in Pacific plate relative plate motion that prompted a more highly convergent Denali fault system (Jicha et al., 2018; Trop et al., 2019).

Southeastward Progression (18–13 Ma)

Wrangell Arc magmatism progressed southeastward from Alaska to Canada from ca. 18 Ma to 13 Ma, based upon new detrital dates in the present

study and previous bedrock dates from volcanic centers and strike-slip basin fills exposed along the Duke River fault (Figs. 16-17). Strike-slip basin development along the Duke River fault is evident from Eocene-Oligocene alluvial fan, fan-delta, and lacustrine strata that are overlain by Miocene (18-13 Ma) lavas and pyroclastic rocks (Fig. 1; Ridgway and DeCelles, 1993; Cole and Ridgway, 1993). The limited spatial distribution of the volcanic rocks along strike-slip faults, with the predominance of small volume, fissure-vent-sourced alkaline volcanic rock compositions, has been attributed to leaky transform volcanism, with magmas being sourced from both mantle affected by subduction (e.g., hydrous mantle wedge like the Alaskan Wrangell Arc) and underlying anhydrous asthenospheric mantle (Skulski et al., 1992; Thorkelson et al., 2011; Brueseke et al., 2019). Age equivalent volcanic centers in the Saint Clare field (Yukon) and Sonya Creek-Rocker Creek area (Alaska) (Fig. 1) appear

to record a spatial transition from chiefly strike-slip to subduction tectonics. Overall, geochemical and isotope variations indicate that many Wrangell volcanic belt products exposed in the Yukon formed via a different melting regime and from different mantle sources than Wrangell Arc magmatism in Alaska. This scenario is consistent with Yukon magmatism occurring along the eastern edge of the subducted slab along the arcuate arc-transform continental margin. We infer that formation of 18–13 Ma volcanic centers along northwest-striking, strike-slip faults in the Yukon reflects oblique convergence and the subduction of oceanic crust along the inboard margin of the Yakutat microplate coeval with dextral-oblique slip on the Denali and Totschunda faults (Figs. 17-18).

We attribute the observed southeastward progression in Wrangell magmatism from Alaska ca. 30-18 Ma to Canada ca. 18-13 Ma (Figs. 16-17) to northwestward translation of the overriding plate via dextral-oblique displacement along the Denali and Totschunda faults (Fig. 18). However, strike-slip translation along the Denali and Totschunda faults alone does not account for the magnitude of southeastward progression in magmatism between 18 Ma to 13 Ma. Given that the pace or orientation of relative plate convergence was relatively consistent along the southern Alaska-western Canada margin between 26 Ma and 13 Ma (Fig. 1; Doubrovine and Tarduno, 2008; Pavlis et al., 2019), we hypothesize that the observed southeastward shift in magmatism also reflects slab steepening, possibly via slab curling related to gravitational pull on the edge of the subducted slab (e.g., Park et al., 2002).

Generally Westward Progression (13 Ma to 6 Ma)

We postulate that slab shallowing (perhaps via uncurling) of the subducted Yakutat slab prompted the observed generally westward progression of volcanic centers and transtensional intra-arc basins along strike-slip faults between 13 Ma and 6 Ma (Totschunda and Duke River faults in Figs. 17–19). Shallowing of the Yakutat slab may reflect slight flattening of the slab edge in response to the progressive subduction of thicker parts of the outboard-thickened, southward Yakutat microplate (Worthington et al., 2012).

Generally Northwestward Progression (6 Ma to 200 ka)

Similar to Richter et al. (1990) and Preece and Hart (2004), we interpret northwestward progression of Wrangell Arc magmatism from 6 Ma to present (Figs. 16–17) as a response to a change in Pacific plate vectors at this time to more rapid (~37%) and with a higher angle of convergence (18° northerly shift) (Fig. 18; Engebretson, 1985; Doubrovine and Tarduno, 2008). Previous geologic and geochronologic studies document a ca. 6 Ma tectonic event across southern Alaska (Fitzgerald et al., 1995; Ridgway et al., 2007; Enkelmann et al., 2008; Allen et al., 2014; Waldien et al., 2018b), which is consistent with a more convergent Pacific/Yakutat-North American interface.

Reduction in Wrangell Arc Magmatism by 200 ka

Richter et al. (1990) postulates a reduction in Wrangell Arc magmatism at ca. 200 ka related to northward progression of the Yakutat microplate. A geophysically imaged slab tear separates eastern (under the Wrangell Arc) and central (under south-central Alaska) segments of the subducted Yakutat slab (Fuis et al., 2008). The spatial association of most <1 Ma Wrangell Arc volcanoes directly southeast of the tear (Fig. 1) and rejuvenated magmatism northwest of the tear in the Alaska Range starting at ca. 1 Ma (Jumbo Dome, Buzzard Maar in the Alaska Range in Fig. 1) implies a change in slab geometry. We posit that these changes in magmatic flux may reflect development of the slab tear at ca. 1 Ma and concurrent with jamming of the trench (Gulick et al., 2013).

Suture Zone Localization of Wrangell Arc Magmatism

Structures are known to facilitate volcanism by acting as conduits (e.g., Gómez-Vasconcelos et al., 2020). The Totschunda-Duke River and Denali faults bracket a Cretaceous suture zone that separates the Insular terranes from inboard terranes in the study area (Figs. 1 and 17-19). The Totschunda and Duke River faults acted as conduits that facilitated magma focusing and rise, as is documented by the alignment of Wrangell Arc volcanoes with these structures (Figs. 1 and 17-19). For example, the 2.4 Ma Euchre Mountain volcano lies along the Totschunda fault and is a classic example of a volcanic edifice forming adjacent to a strike-slip fault (Figs. 3 and 17; Keast et al., 2016). Given that the suture zone has been translated ~180 km along the eastern Denali fault since 30 Ma (Fig. 18), and much of the Wrangell Arc magmatism is away from these faults (Fig. 17), the presence of these long-lived suture zone faults alone does not explain localization of Wrangell Arc magmatism within and adjacent to the Insular terranes-North America suture zone. The suture zone is defined by lithologic and thickness variations of the crust (Fitzgerald et al., 2014), which include crustal thickness variations across the suture-bounding Denali, Totschunda, and Duke River faults (Fig. 19). Throughout its 30 m.y. evolution, Wrangell Arc magmatism never migrated into crust north of the Denali fault (Yukon-Tanana terrane in Figs. 18-19). Given that the trench outboard (south) of the Wrangell Arc trends essentially the same as the eastern Denali fault, the distance between the Wrangell Arc and the trench was relatively constant (~300 km) during translation of the Insular terranes-North America suture zone along the Denali fault during the 30 Ma history of Wrangell Arc magmatism (Fig. 18).

Late Cretaceous-Paleogene arc magmatism in the Western and Central Alaska Range (Fig. 1) was similarly localized along the Insular terranes-North America suture zone (Jones et al., 2021), and crustal variations within the suture zone likely played a hydrostatic role in flattening the underlying slab(s) regardless of slab characteristics (Trop et al., 2019). We posit that similar geodynamic processes prompted the dewatering depth zone along the eastern edge of the subducted Yakutat slab to track with the migrating upper plate suture zone until

6 Ma. After the increase in the Pacific–North America plates' convergence rate at ca. 6 Ma (Doubrovine and Tarduno, 2008), the leading lateral (northeastern) edge of the Yakutat slab was apparently less influenced by crustal thickness variations, and magmatism drifted away from the suture zone proper.

In summary, the reconstructed spatial-temporal evolution of arc-transform magmatism documented in the Wrangell Arc is attributed to dextral translation of the overriding plate, changes in the subducting slab geometry, variations in relative plate convergence, and the influence of a suture zone and intra-arc, strike-slip faults on magma-surface flux.

Voluminous Wrangell Arc-Transform Magmatism

Based on the enormous sizes of Wrangell Arc volcanoes, melt production along the arc-transform margin was voluminous (Item S1 [footnote 1]; Richter et al., 2006). We attribute this scenario partly to the flat slab setting and upwelling along the edge of the subducting Yakutat slab (Brueseke et al., 2019) as well as to the outsized surface area presented for dehydration due to the low angle of slab dip (Figs. 1 and 19) (Arce et al., 2020). The massive sizes of Wrangell Arc volcanoes also must reflect common depths of magma production, melt extraction, and similar transcrustal magmatic systems (Cashman et al., 2017; Jackson et al., 2018). The slab-edge setting helped to focus voluminous magmatism and led to the formation of large volcanoes and is similar to magmatism documented along subduction-transform edge propagator (STEP) faults along slab tears (Cocchi et al., 2017). Available geologic and geophysical data sets indicate a similar general type of mantle focusing, where toroidal and poloidal flow of the underlying mantle has occurred along the edge of the Yakutat slab (Jadamec and Billen, 2010). Although STEP faults have not been recognized in the Wrangell Arc, geophysical data sets indicate the presence of a significant slab tear along its northwestern edge (Fuis et al., 2008; Mann et al., 2020). Voluminous slab-edge magmatism characterized by complex spatial-temporal shifts documented in the present study may be a previously overlooked hallmark of arc-transform margins, especially for those influenced by flat-slab subduction.

CONCLUSIONS

The Wrangell volcanic belt in eastern Alaska and the Yukon provides an archetypical environ in which to examine the relations between magmatism, deformation, and plate interactions along an active continental arc-transform junction. Abundant new DZ U-Pb and DARL 40Ar-39Ar dates from modern rivers and bedrock dates demonstrate that the Wrangell Arc was continuously active from ca. 30 Ma to present. Palinspastic reconstruction of the arc along regional strike-slip faults (Figs. 17–18) allows the spatial migration of arc magmatism during its evolution to be documented. First-order findings from our study are:

DARL dates provide a more robust record of the generally mafic <30 Ma
 Wrangell Arc than DZ dates, which better document older episodes of

- more felsic magmatism that shaped the crust and match Paleozoic–Mesozoic magmatic flare-ups documented along the Cordilleran margin.
- (2) Wrangell Arc magmatism was emplaced within or adjacent to a suture zone separating the Insular terranes to the south and the Yukon-Tanana terrane to the north. The spatial association of magmatism with the suture zone indicates localization of magmatism in response to upper plate crustal heterogeneities and pre-existing structural zones that served as active magma conduits.
- (3) The history of magmatism, combined with regional constraints, is interpreted to be most consistent with the following tectonic model (Figs. 17-19). The Wrangell Arc is interpreted to have initiated at ca. 30-17 Ma in response to northward convergence and subduction of the lithosphere of the oceanic plateau along the inboard northeastern lateral edge of the Yakutat microplate. The Totschunda fault, an intraarc, strike-slip fault, was an active conduit for magmas during this time. Southeastward progression of magmatism from ca. 17 Ma to 10 Ma is attributable to strike-slip translation of the Wrangell Arc and slab steepening/curling. Magmatism was focused along the Duke River fault, which was an active conduit for magma ascent. Generally westward and northwestward shifts in magmatism from ca. 13 Ma to 6 Ma reflect translation of the Wrangell Arc along strike-slip faults and slab shallowing/uncurling during the subduction of progressively thicker parts of the outboard (southward) thickened Yakutat microplate. A previously documented increase in plate convergence rate and angle at ca. 6 Ma prompted the northwestward migration of magmatism from ca. 6 Ma to Present and was accompanied by translation of older sectors of the Wrangell Arc along the rejuvenated Totschunda fault.
- (4) The exceptional volume of Wrangell Arc volcanoes is attributed to shallow subduction-related flux melting and slab edge melting driven by asthenospheric upwelling along the lateral edge of the Yakutat flat slab.
- (5) The observed spatial age patterns of magmatism demonstrate that the Wrangell Arc varied from ~110 km to ~190 km in length, which is substantially shorter than most modern arcs. The short arc length reflects subduction of a relatively short slab along the lateral edge of the shallowly subducting Yakutat microplate within an arc-transform junction, which is unlike longer arcs that formed along extensive trenches.
- (6) Arc-transform junctions may be identified in the geologic record by the presence of short arc lengths with voluminous magmatism, volcanic products with calc-alkaline to transitional geochemical signatures, and complex age patterns resulting from strike-slip displacements and changes in plate interaction/slab geometry.

ACKNOWLEDGMENTS

This research was supported by grants from the National Science Foundation to M.E. Brueseke (EAR-1450689), J.A. Benowitz (EAR-1450730), and J.M. Trop (EAR-1450687). Samples were collected under permits from Wrangell-St. Elias National Park and Preserve. Special thanks to S. Berkelhammer, B. Bliss, K. Davis, N. Geisler, D. Koepp, P. Layer, B. Morter, B. Mortetti, M. Pecha,

Devil's Mountain Lodge, Last Frontier Air, Soloy Air, and Wrangell Mountain Air for assistance. J.M. Trop, J.A. Benowitz, and M.E. Brueseke collected and processed samples; J.M. Trop analyzed detrial zircons, J.A. Benowitz analyzed volcanic lithics, and C.S. Kirby conducted GIS analyses. All authors contributed to the manuscript. Feedback from two anonymous reviewers helped us to revise the manuscript.

REFERENCES CITED

- Albanese, M., 1980, The geology of three extrusive bodies in central Alaska Range [M.S. thesis]: University of Alaska Fairbanks, 104 p.
- Aleinikoff, J.N., Dusel-Bacon, C., and Foster, H.L., 1981, Geochronologic studies in the Yukon-Tanana Upland, east-central Alaska, in accomplishments during 1979: Geological Survey Circular, v. 823-B, p. B34–B37.
- Aleinikoff, J.N., Foster, H.L., Nokleberg, W.J., and Dusel-Bacon, C., 1984, Isotopic evidence from detrital zircons for Early Proterozoic crustal materials, east-central Alaska, in accomplishments during 1981: Geological Survey Circular, v. 868, p. 43–45.
- Aleinikoff, J.N., Dusel-Bacon, C., and Foster, H.L., 1986, Geochronology of augen gneiss and related rocks, Yukon-Tanana terrane, east-central Alaska: Geological Society of America Bulletin, v. 97, p. 626–637, https://doi.org/10.1130/0016-7606(1986)97<626:GOAGAR>2.0.CO;2.
- Allam, A.A., Schulte-Pelkum, V., Ben-Zion, Y., Tape, C., Ruppert, N., and Ross, Z.E., 2017, Ten kilometer vertical Moho offset and shallow velocity contrast along the Denali fault zone from double-difference tomography, receiver functions, and fault zone head waves: Tectonophysics, v. 721, p. 56–69, https://doi.org/10.1016/j.tecto.2017.09.003.
- Allen, W.K., 2016, Miocene-Pliocene strike-slip basin development along the Denali fault system in the eastern Alaska range: Chronostratigraphy and provenance of the McCallum formation and implications for displacement [M.S. thesis]: West Lafayette, Indiana, USA, Purdue University, 162 p., https://docs.lib.purdue.edu/open_access_theses/830.
- Allen, W.K., Ridgway, K.D., Benowitz, J.A., Waldien, T.S., and Roeske, S.M., 2014, Neogene transpressional basin development along the Denali Fault System in the Eastern Alaska Range: The stratigraphy of the McCallum Basin and implications for displacement along the Denali fault system: Geological Society of America Abstracts with Programs, v. 46, no. 6, p. 364.
- Amidon, W.H., Burbank, D.W., and Gehrels, G.E., 2005, Construction of detrital mineral populations: Insights from mixing of U-Pb zircon ages in Himalayan rivers: Basin Research, v. 17, p. 463–485, https://doi.org/10.1111/j.1365-2117.2005.00279.x.
- Andronikov, A.V., and Mukasa, S.B., 2010, 40Ar/39Ar eruption ages and geochemical characteristics of Late Tertiary to Quaternary intraplate and arc-related lavas in interior Alaska: Lithos, v. 115, p. 1–14, https://doi.org/10.1016/j.lithos.2009.11.002.
- Arboit, F., Min, M., Chew, D., Mitchell, A., Drost, K., Badenszki, E., and Daly, J.S., 2020, Constraining the links between the Himalayan belt and the Central Myanmar Basins during the Cenozoic:

 An integrated multi-proxy detrital geochronology and trace-element geochemistry study: Geoscience Frontiers, v. 12, p. 657–676, https://doi.org/10.1016/j.gsf.2020.05.024.
- Arce, J.L., Ferrari, L., Morales-Casique, E., Vasquez-Serrano, A., Arroyo, S.M., Layer, P.W., Benowitz, J., and López-Martínez, M., 2020, Early Miocene arc volcanism in the Mexico City Basin: Inception of the Trans-Mexican Volcanic Belt: Journal of Volcanology and Geothermal Research, v. 408, no. 107104, https://doi.org/10.1016/j.jvolgeores.2020.107104.
- Athey, J.E., Newberry, R.J., Werdon, M.B., Freeman, L.K., Smith, R.L., and Szumigala, D.J., 2006, Bedrock geologic map of the Liberty Bell area, Fairbanks A-4 Quadrangle, Bonnifield mining district, Alaska: Alaska Division of Geological & Geophysical Surveys Report of Investigation 2006–2 v. 1.0.1, scale 1:50,000, 1 sheet, 98 p.
- Axen, G.J., van Wijk, J.W., and Currie, C.A., 2018, Basal continental mantle lithosphere displaced by flatslab subduction: Nature Geoscience, v. 11, p. 961–964, https://doi.org/10.1038/s41561-018-0263-9.
- Baldwin, S.L., Fitzgerald, P.G., and Webb, L.E., 2012, Tectonics of the New Guinea region: Annual Review of Earth and Planetary Sciences, v. 40, p. 495–520, https://doi.org/10.1146/annurev -earth-040809-152540.
- Bauer, M.A., Pavlis, G.L., and Landes, M., 2014, Subduction geometry of the Yakutat terrane, south-eastern Alaska: Geosphere, v. 10, p. 1161–1176, https://doi.org/10.1130/GES00852.1.
- Benowitz, J., and Addison, J., 2017, Developing a tephra database for IODP Sites U1417 and U1418: Late Miocene to Present evolution of eruptive volcanism along the Gulf of Alaska: Geological Society of America Abstracts with Programs, v. 49, no. 4, https://doi.org/10.1130/abs/2017CD-292892.

- Benowitz, J.A., Layer, P.W., Armstrong, P., Perry, S.E., Haeussler, P.J., Fitzgerald, P.G., and Van-Laningham, S., 2011, Spatial variations in focused exhumation along a continental-scale strike-slip fault: The Denali fault of the eastern Alaska Range: Geosphere, v. 7, p. 455–467, https://doi.org/10.1130/GES00589.1.
- Benowitz, J.A., Haeussler, P.J., Layer, P.W., O'Sullivan, P.B., Wallace, W.K., and Gillis, R.J., 2012a, Cenozoic tectono-thermal history of the Tordrillo Mountains, Alaska: Paleocene-Eocene ridge subduction, decreasing relief, and late Neogene faulting: Geochemistry, Geophysics, Geosystems, V. 13, no. 4, https://doi.org/10.1029/2011GC003951.
- Benowitz, J.A., Vansant, G., Roeske, S., Layer, P.W., Hults, C.P., and O'Sullivan, P., 2012b, Geochronological constraints on the Eocene to present slip rate history of the eastern Denali fault system: Geological Society of America Abstracts with Programs, v. 44, no. 7, p. 634.
- Benowitz, J.A., Layer, P.W., and Vanlaningham, S., 2014, Persistent long-term (c. 24 Ma) exhumation in the Eastern Alaska Range constrained by stacked thermochronology, in Jourdan, F., Mark, D.F., and Verati, C., eds., Advances in 40Ar/30Ar Dating: From Archaeology to Planetary Sciences: Geological Society, London, Special Publication 378, p. 225–243, https://doi.org/10.1144/SP378.12.
- Benowitz, J.A., Davis, K., and Roeske, S., 2019, A river runs through it both ways across time: **0Ar/**2Ar detrital and bedrock muscovite geochronology constraints on the Neogene paleodrainage history of the Nenana River system, Alaska Range: Geosphere, v. 15, p. 682–701, https://doi.org/10.1130/GES01673.1.
- Beranek, L.P., van Staal, C.R., McClelland, W.C., Joyce, N., and Israel, S., 2014, Late Paleozoic assembly of the Alexander-Wrangellia-Peninsular composite terrane, Canadian and Alaskan Cordillera: Geological Society of America Bulletin, v. 126, p. 1531–1550, https://doi.org /10.130/31066.1
- Beranek, L.P., McClelland, W.C., van Staal, C.R., Israel, S., and Gordee, S.M., 2017, Late Jurassic flare-up of the Coast Mountains arc system, NW Canada, and dynamic linkages across the northern Cordilleran orogeny: Tectonics. v. 36. p. 877–901. https://doi.org/10.1002/2016TC004254.
- Berkelhammer, S.E., Brueseke, M.E., Benowitz, J.A., Trop, J.M., Davis, K., Layer, P.W., and Weber, M., 2019, Geochemical and geochronological records of tectonic changes along a flat-slab arc-transform junction: Circa 30 Ma to ca. 19 Ma Sonya Creek volcanic field, Wrangell Arc, Alaska: Geosphere, v. 15, p. 1508–1538, https://doi.org/10.1130/GES02114.1
- Bishop, B.T., Beck, S.L., Zandt, G., Wagner, L., Long, M., Antonijevic, S.K., Kumar, A., and Tavera, H., 2017, Causes and consequences of flat-slab subduction in southern Peru: Geosphere, v. 13, p. 1392–1407, https://doi.org/10.1130/GES01440.1.
- Bootes, N., Enkelmann, E., and Lease, R., 2019, Late Miocene to Pleistocene source to sink record of exhumation and sediment routing in the Gulf of Alaska from detrital zircon fission-track and U-Pb double dating: Tectonics, v. 38, p. 2703–2726, https://doi.org/10.1029/2019TC005497.
- Box, S.E., Karl, S.M., Jones, J.V., III, Bradley, D.C., Haeussler, P.J., and O'Sullivan, P.B., 2019, Detrital zircon geochronology along a structural transect across the Kahiltna assemblage in the western Alaska Range: Implications for emplacement of the Alexander-Wrangellia-Peninsular terrane against North America: Geosphere, v. 15, p. 1774–1808, https://doi.org/10 .1130/GES02060.1
- Brennan, P.R., and Ridgway, K.D., 2015, Detrital zircon record of Neogene exhumation of the central Alaska Range: A far-field upper plate response to flat-slab subduction: Geological Society of America Bulletin, v. 127, p. 945–961, https://doi.org/10.1130/B31164.1.
- Brueseke, M.E., Benowitz, J.A., Trop, J.M., Davis, K.N., Berkelhammer, S.E., Layer, P.W., and Morter, B.K., 2019, The Alaska Wrangell Arc: ~30 m.y. of subduction-related magmatism along a still active arc-transform junction: Terra Nova, v. 31, p. 59–66, https://doi.org/10.1111/ter.12369.
- Bush, M.A., Saylor, J.E., Horton, B.K., and Nie, J., 2016, Growth of the Qaidam Basin during Cenozoic exhumation in the northern Tibetan Plateau: Inferences from depositional patterns and multiproxy detrital provenance signatures: Lithosphere, v. 8, p. 58–82, https://doi.org /10.1130/L449.1.
- Cameron, C.E., 2005, Latitudes and longitudes of volcanoes in Alaska: State of Alaska, Alaska Division of Geological & Geophysical Surveys, Raw Data File 2005–3.
- Cameron, C.E., Nye, C., Bull, K.F., and Woods, R.E.F., 2015, Jumbo Dome, Interior Alaska: Wholerock major-and trace-element analyses: State of Alaska, Department of Natural Resources, Division of Geological & Geophysical Surveys, Raw Data File 2015-14.
- Capaldi, T.N., Horton, B.K., McKenzie, N.R., Stockli, D.F., and Odlum, M.L., 2017, Sediment provenance in contractional orogens: The detrital zircon record from modern rivers in the Andean fold-thrust belt and foreland basin of western Argentina: Earth and Planetary Science Letters, v. 479, p. 83–97, https://doi.org/10.1016/j.epsl.2017.09.001.

- Capaldi, T.N., Horton, B.K., McKenzie, N.R., Mackaman-Lofland, C., Stockli, D.F., Ortiz, G., and Alvarado, P., 2020, Neogene retroarc foreland basin evolution, sediment provenance, and magmatism in response to flat slab subduction, western Argentina: Tectonics, v. 39, no. e2019TC005958, https://doi.org/10.1029/2019TC005958.
- Cashman, K.V., Sparks, R.S.J., and Blundy, J.D., 2017, Vertically extensive and unstable magmatic systems: A unified view of igneous processes: Science, v. 355, https://doi.org/10.1126/science.aag3055.
- Cawood, P.A., Hawkesworth, C.J., and Dhuime, B., 2012, Detrital zircon record and tectonic setting: Geology, v. 40, p. 875–878, https://doi.org/10.1130/G32945.1.
- Cocchi, L., Passaro, S., Tontini, F.C., and Ventura, G., 2017, Volcanism in slab tear faults is larger than in island-arcs and back-arcs: Nature Communications, v. 8, no. 1451, https://doi.org/10.1038/s41467-017-01626-w.
- Cole, R.B., and Ridgway, K.D., 1993, The influence of volcanism on fluvial depositional systems in a Cenozoic strike-slip basin, Denali fault system, Yukon Territory, Canada: Journal of Sedimentary Research, v. 63, p. 152–166.
- Cooper, L.B., Plank, T., Arculus, R.J., Hauri, E.H., Hall, P.S., and Parman, S.W., 2010, High-Ca boninites from the active Tonga Arc: Journal of Geophysical Research: Solid Earth, v. 115, https://doi.org/10.1029/2009JB006367.
- Day, W.C., O'Neill, J.M., Dusel-Bacon, C., Aleinikoff, J.N., and Siron, C.R., 2014, Geologic map of the Kechumstuk fault zone in the Mount Veta area, Fortymile mining district, east-central Alaska: U.S. Geological Survey, Investigation Series Map 3291, scale 1:63,360, 1 plate.
- DeCelles, P.G., Ducea, M.N., Kapp, P., and Zandt, G., 2009, Cyclicity in Cordilleran orogenic systems: Nature Geoscience, v. 2, p. 251–257, https://doi.org/10.1038/ngeo469.
- DeCelles, P.G., Zandt, G., Beck, S.L., Currie, C.A., Ducea, M.N., Kapp, P., Gehrels, G.E., Carrapa, B., Quade, J., and Schoenbohm, L.M., 2015, Cyclical orogenic processes in the central Cenozoic Andes, in DeCelles, P.G., Ducea, M.N., Carrapa, B., and Kapp, P.A. eds., Geodynamics of a Cordilleran Orogenic System: The Central Andes of Argentina and Northern Chile: Geological Society of America Memoir 212, p. 459–490, https://doi.org/10.1130/2015.1212(22).
- de Silva, S.L., Riggs, N.R., and Barth, A.P., 2015, Quickening the pulse: Fractal tempos in continental arc magmatism: Elements, v. 11, p. 113–118, https://doi.org/10.2113/gselements.11.2.113.
- Dickinson, W.R., 2008, Impact of differential zircon fertility of granitoid basement rocks in North America on age populations of detrital zircons and implications for granite petrogenesis: Earth and Planetary Science Letters, v. 275, p. 80–92, https://doi.org/10.1016/j.epsl.2008.08.003.
- Di Giulio, A., Ronchi, A., Sanfilippo, A., Balgord, E.A., Carrapa, B., and Ramos, V.A., 2017, Cretaceous evolution of the Andean margin between 36° S and 40° S latitude through a multi-proxy provenance analysis of Neuquén Basin strata (Argentina): Basin Research, v. 29, p. 284–304, https://doi.org/10.1111/bre.12176.
- Dodds, C.J., and Campbell, R.B., 1988, Potassium-Argon Ages of Mainly Intrusive Rocks in the Saint Elias Mountains, Yukon and British Columbia: Geological Survey of Canada, Paper 87–16, 43 p., https://doi.org/10.4095/126100.
- Doubrovine, P.V., and Tarduno, J.A., 2008, A revised kinematic model for the relative motion between Pacific oceanic plates and North America since the Late Cretaceous: Journal of Geophysical Research: Solid Earth, v. 113, p. 1–20.
- Ducea, M.N., and Barton, M.D., 2007, Igniting flare-up events in Cordilleran arcs: Geology, v. 35, p. 1047–1050, https://doi.org/10.1130/G23898A.1.
- Dusel-Bacon, C., and Williams, I.S., 2009, Evidence for prolonged mid-Paleozoic plutonism and ages of crustal sources in east-central Alaska from SHRIMP U-Pb dating of syn-magmatic, inherited, and detrital zircon: Canadian Journal of Earth Sciences, v. 46, p. 21–39, https://doi .org/10.1139/E09-005.
- Dusel-Bacon, C., Hopkins, M.J., Mortenson, J.K., Dashevsky, S.S., Bressler, J.R., and Day, W.C., 2006, Paleozoic tectonic and metallogenic evolution of the pericratonic rocks of east-central Alaska and adjacent Yukon Territory, in Colpron, M., and Nelson, J., eds., Paleozoic Evolution and Metallogeny of Pericratonic Terranes at the Ancient Pacific Margin of North America, Canadian and Alaskan Cordillera: Geological Association Canada Special Paper 45, p. 25–74.
- Eberhart-Phillips, D., Christensen, D.H., Brocher, T.M., Hansen, R., Ruppert, N.A., Haeussler, P.J., and Abers, G.A., 2006, Imaging the transition from Aleutian subduction to Yakutat collision in central Alaska, with local earthquakes and active source data: Journal of Geophysical Research: Solid Earth, v. 111, p. 1–31.
- Elliott, J.L., Larsen, C.F., Freymueller, J.T., and Motyka, R.J., 2010, Tectonic block motion and glacial isostatic adjustment in southeast Alaska and adjacent Canada constrained by GPS measurements: Journal of Geophysical Research: Solid Earth, v. 115, https://doi.org/10.1029/2009JB007139.

- Engebretson, D.C., Cox, A., and Gordon, R.G., 1985, Relative Motions Between Oceanic and Continental Plates in the Pacific Basin: Geological Society of America Special Paper 206, https://doi.org/10.1130/SPE206-p1.
- Enkelmann, E., Garver, J.I., and Pavlis, T.L., 2008, Rapid exhumation of ice-covered rocks of the Chugach–St. Elias orogen, Southeast Alaska: Geology, v. 36, p. 915–918, https://doi.org/10 .1130/G2252A.1.
- Enkelmann, E., Koons, P.O., Pavlis, T.L., Hallet, B., Barker, A., Elliott, J., Garver, J.I., Gulick, S.P.S., Headley, R.M., Pavlis, G.L., Ridgway, K.D., Ruppert, N., and Van Avendonk, H.J.A., 2015a, Cooperation among tectonic and surface processes in the St. Elias Range, Earth's highest coastal mountains: Geophysical Research Letters, v. 42, p. 5838–5846, https://doi.org/10.1002/2015GL064727.
- Enkelmann, E., Valla, P.G., and Champagnac, J., 2015b, Low-temperature thermochronology of the Yakutat plate corner, St. Elias Range (Alaska): Bridging short-term and long-term deformation: Quaternary Science Reviews, v. 113, p. 23–38, https://doi.org/10.1016/j.quascirev.2014.10.019.
- Fan, M., and Carrapa, B., 2014, Late Cretaceous–early Eocene Laramide uplift, exhumation, and basin subsidence in Wyoming: Crustal responses to flat slab subduction: Tectonics, v. 33, p. 509–529, https://doi.org/10.1002/2012TC003221.
- Fasulo, C.R., 2019, Sedimentary record of tectonic growth along a convergent margin: Insights from detrital zircon geochronology of Mesozoic sedimentary basins and modern rivers in south-central Alaska [M.S. thesis]: West Lafayette, Indiana, USA, Purdue University, 235 p.
- Fasulo, C.R., Ridgway, K.D., and Trop, J.M., 2020, Detrital zircon geochronology and Hf isotope geochemistry of Mesozoic sedimentary basins in south-central Alaska: Insights into regional sediment transport, basin development, and tectonics along the NW Cordilleran margin: Geosphere, v. 16, p. 1125–1152, https://doi.org/10.1130/GES02221.1.
- Ferrari, L., López-Martínez, M., Aguirre-Díaz, G., and Carrasco-Núñez, G., 1999, Space-time patterns of Cenozoic arc volcanism in central Mexico: From the Sierra Madre Occidental to the Mexican Volcanic Belt: Geology, v. 27, p. 303–306, https://doi.org/10.1130/0091-7613(1999)027 <0303:STPOCA>2.3.CO;2.
- Finzel, E.S., and Ridgway, K.D., 2017, Links between sedimentary basin development and Pacific Basin plate kinematics recorded in Jurassic to Miocene strata on the western Alaska Peninsula: Lithosphere, v. 9, p. 58–77, https://doi.org/10.1130/L592.1.
- Finzel, E.S., Trop, J.M., Ridgway, K.D., and Enkelmann, E., 2011, Upper plate proxies for flatslab subduction processes in southern Alaska: Earth and Planetary Science Letters, v. 303, p. 348–360, https://doi.org/10.1016/j.epsl.2011.01.014.
- Finzel, E.S., Enkelmann, E., Falkowski, S., and Hedeen, T., 2016, Long-term fore-arc basin evolution in response to changing subduction styles in southern Alaska: Tectonics, v. 35, p. 1735–1759, https://doi.org/10.1002/2016TC004171.
- Fitch, T.J., 1972, Plate convergence, transcurrent faults, and internal deformation adjacent to southeast Asia and the western Pacific: Journal of Geophysical Research, v. 77, p. 4432–4460, https://doi.org/10.1029/JB077i023p04432.
- Fitzgerald, P.G., Sorkhabi, R.B., Redfield, T.F., and Stump, E., 1995, Uplift and denudation of the central Alaska Range: A case study in the use of apatite fission track thermochronology to determine absolute uplift parameters: Journal of Geophysical Research: Solid Earth, v. 100, p. 20,175–20,191, https://doi.org/10.1029/95JB02150.
- Fitzgerald, P.G., Roeske, S.M., Benowitz, J.A., Riccio, S.J., Perry, S.E., and Armstrong, P.A., 2014, Alternating asymmetric topography of the Alaska range along the strike-slip Denali fault: Strain partitioning and lithospheric control across a terrane suture zone: Tectonics, v. 33, p. 1519–1533, https://doi.org/10.1002/2013TC003432.
- Fuis, G.S., Moore, T.E., Plafker, G., Brocher, T.M., Fisher, M.A., Mooney, W.D., Nokleberg, W.J., Page, R.A., Beaudoin, B.C., Christensen, N.I., and Levander, A.R., 2008, Trans-Alaska Crustal Transect and continental evolution involving subduction underplating and synchronous foreland thrusting: Geology, v. 36, p. 267–270, https://doi.org/10.1130/G24257A.1.
- Gehrels, G., 2014, Detrital zircon U-Pb geochronology applied to tectonics: Annual Review of Earth and Planetary Sciences, v. 42, p. 127–149, https://doi.org/10.1146/annurev-earth-050212-124012.
- Gehrels, G.E., 2000, Reconnaissance geology and U-Pb geochronology of the western flank of the Coast Mountains between Juneau and Skagway, southeastern Alaska, in Stowell, H.H., and McClelland, W.C., eds., Tectonics of the Coast Mountains, Southeastern Alaska and British Columbia: Geological Society of America Special Paper 343, p. 213–234, https://doi.org/10.1130/0-8137-2343-4.213.
- Gehrels, G.E., et al., 2009, U-Th-Pb geochronology of the Coast Mountains batholith in north-coastal British Columbia: Constraints on age, petrogenesis, and tectonic evolution: Geological Society of America Bulletin, v. 121, p. 1341–1361, https://doi.org/10.1130/B26404.1.

- Giambiagi, L., Álvarez, P.P., Creixell, C., Mardonez, D., Murillo, I., Velásquez, R., Lossada, A., Suriano, J., Mescua, J., and Barrionuevo, M., 2017, Cenozoic shift from compression to strike-slip stress regime in the High Andes at 30° S, during the shallowing of the slab: Implications for the El Indio/Tambo mineral district: Tectonics, v. 36, p. 2714–2735, https://doi.org/10.1002/2017TC004608.
- Girardi, J.D., Patchett, P.J., Ducea, M.N., Gehrels, G.E., Cecil, M.R., Rusmore, M.E., Woodsworth, G.J., Pearson, D.M., Manthei, C., and Wetmore, P., 2012, Elemental and isotopic evidence for granitoid genesis from deep-seated sources in the Coast Mountains batholith, British Columbia: Journal of Petrology, v. 53, p. 1505–1536, https://doi.org/10.1093/petrology/egs024.
- Gómez-Vasconcelos, M.G., Luis Macías, J., Avellán, D.R., Sosa-Ceballos, G., Garduño-Monroy, V.H., Cisneros-Máximo, G., Layer, R.W., Benowitz, J., López-Loera, H., López, F.M., and Perton, M., 2020, The control of preexisting faults on the distribution, morphology, and volume of monogenetic volcanism in the Michoacán-Guanajuato Volcanic Field: Geological Society of America Bulletin, v. 132, p. 2455–2474, https://doi.org/10.1130/835397.1
- Graham, G., Kelley, K., Holm-Denoma, C., Ayuso, R., Kokaly, R., Hoefen, T., and Selby, D., 2016, Geochronology and Nd-Sr-Pb isotopic compositions of early intrusions and associated porphyry Cu deposits in eastern Alaska: Abstract 4858 presented at 35th International Geological Congress, Capetown, South Africa, 27 August–4 September, www.americangeosciences.org /sites/default/files/igc/4858.pdf.
- Grebennikov, A.V., and Khanchuk, A.I., 2020, Pacific-type transform and convergent margins: Igneous rocks, geochemical contrasts and discriminant diagrams: International Geology Review, v. 63, p. 1–29.
- Greene, A.R., Scoates, J.S., Weis, D., Nixon, G.T., and Kieffer, B., 2009, Melting history and magmatic evolution of basalts and picrites from the accreted Wrangellia oceanic plateau, Vancouver Island, Canada: Journal of Petrology, v. 50, p. 467–505, https://doi.org/10.1093/petrology/egp008.
- Greene, A.R., Scoates, J.S., Weis, D., Katvala, E.C., Israel, S., and Nixon, G.T., 2010, The architecture of oceanic plateaus revealed by the volcanic stratigraphy of the accreted Wrangellia oceanic plateau: Geosphere, v. 6, p. 47–73, https://doi.org/10.1130/GES00212.1.
- Guillaume, B., Martinod, J., and Espurt, N., 2009, Variations of slab dip and overriding plate tectonics during subduction: Insights from analogue modelling: Tectonophysics, v. 463, p. 167–174, https://doi.org/10.1016/j.tecto.2008.09.043.
- Gulick, S.P.S., Reece, R.S., Christeson, G.L., Van Avendonk, H., Worthington, L.L., and Pavlis, T.L., 2013, Seismic images of the Transition fault and the unstable Yakutat–Pacific–North American triple junction: Geology, v. 41, p. 571–574, https://doi.org/10.1130/G33900.1.
- Gulick, S.P.S., Jaeger, J.M., Mix, A.C., Asahi, H., Bahlburg, H., Belanger, C.L., Berbel, G.B., Childress, L., Cowan, E., Drab, L., and Forwick, M., 2015, Mid-Pleistocene climate transition drives net mass loss from rapidly uplifting St. Elias Mountains, Alaska: Proceedings of the National Academy of Sciences of the United States of America, v. 112, p. 15042–15047, https://doi.org/10.1073/pnas.1512549112.
- Gutscher, M.A., Spakman, W., Bijwaard, H., and Engdahl, E.R., 2000, Geodynamics of flat subduction: Seismicity and tomographic constraints from the Andean margin: Tectonics, v. 19, p. 814–833, https://doi.org/10.1029/1999TC001152.
- Haeussler, P.J., Matmon, A., Schwartz, D.P., and Seitz, G.G., 2017, Neotectonics of interior Alaska and the late Quaternary slip rate along the Denali fault system: Geosphere, v. 13, p. 1445–1463, https://doi.org/10.1130/GES01447.1.
- Hampton, B.A., Ridgway, K.D., and Gehrels, G.E., 2010, A detrital record of Mesozoic island arc accretion and exhumation in the North American Cordillera: U-Pb geochronology of the Kahiltna basin, southern Alaska: Tectonics, v. 29, no. 4, https://doi.org/10.1029/2009TC002544.
- Harrison, R.W., Newell, W.L., Batihanlı, H., Panayides, I., McGeehin, J.P., Mahan, S.A., Özhür, A., Tsiolakis, E., and Necdet, M., 2004, Tectonic framework and Late Cenozoic tectonic history of the northern part of Cyprus: Implications for earthquake hazards and regional tectonics: Journal of Asian Earth Sciences, v. 23, p. 191–210, https://doi.org/10.1016/S1367-9120(03)00095-6.
- Haschke, M., Gunther, A., Melnick, D., Echtler, H., Reutter, K.J., Scheuber, E., and Oncken, O., 2006, Central and southern Andean tectonic evolution inferred from arc magmatism, in Oncken, O., Chong, G., Franz, G., Giese, P., Götze, H.-J., Ramos, H.-J., Strecker, M.R., and Wigger, P., eds., The Andes—Active Subduction Orogeny: Frontiers in Earth Sciences: Berlin, Springer-Verlag, v. 1, p. 337–353, https://doi.org/10.1007/978-3-540-48684-8, 16.
- Haynie, K.L., and Jadamec, M.A., 2017, Tectonic drivers of the Wrangell block: Insights on fore-arc sliver processes from 3-D geodynamic models of Alaska: Tectonics, v. 36, p. 1180–1206, https:// doi.org/10.1002/2016TC004410.
- Israel, S., Beranek, L., Friedman, R.M., and Crowley, J.L., 2014, New ties between the Alexander terrane and Wrangellia and implications for North America Cordilleran evolution: Lithosphere, v. 6, p. 270–276, https://doi.org/10.1130/L364.1.

- Jackson, M.D., Blundy, J., and Sparks, S., 2018, Chemical differentiation, cold storage and remobilization of magma in the Earth's crust: Nature, v. 564, p. 405–409, https://doi.org/10.1038 /s41586-018-0746-2.
- Jadamec, M.A., and Billen, M.I., 2010, Reconciling surface plate motions with rapid three-dimensional mantle flow around a slab edge: Nature, v. 465, p. 338–341, https://doi.org/10.1038/nature09053.
- Jensen, B.J., Pyne-O'Donnell, S., Plunkett, G., Froese, D.G., Hughes, P.D., Sigl, M., McConnell, J.R., Amesbury, M.J., Blackwell, P.G., van den Bogaard, C., and Buck, C.E., 2014, Transatlantic distribution of the Alaskan White River ash: Geology, v. 42, p. 875–878, https://doi.org/10.1130/G35945.1.
- Jicha, B.R., Scholl, D.W., Singer, B.S., Yogodzinski, G.M., and Kay, S.M., 2006, Revised age of Aleutian island arc formation implies high rate of magma production: Geology, v. 34, p. 661–664, https://doi.org/10.1130/G22433.1.
- Jicha, B.R., Garcia, M.O., and Wessel, P., 2018, Mid-Cenozoic Pacific plate motion change: Implications for the northwest Hawaiian Ridge and circum-Pacific: Geology, v. 46, p. 939–942, https://doi.org/10.1130/G45175.1.
- Jones, J.V., Todd, E., Box, S.E., Haeussler, P.J., Holm-Denoma, C.S., Karl, S.M., Graham, G.E., Bradley, D.C., Kylander-Clark, A.R., Friedman, R.M., and Layer, P.W., 2021, Cretaceous to Oligocene magmatic and tectonic evolution of the western Alaska Range: Insights from U-Pb and 40Ar/59Ar geochronology: Geosphere, v. 17, 118–153, https://doi.org/10.1130/GES02303.1.
- Kapp, P., and DeCelles, P.G., 2019, Mesozoic–Cenozoic geological evolution of the Himalayan–Tibetan orogen and working tectonic hypotheses: American Journal of Science, v. 319, p. 159–254, https://doi.org/10.2475/03.2019.01.
- Kay, S.M., and Mpodozis, C., 2002, Magmatism as a probe to the Neogene shallowing of the Nazca plate beneath the modern Chilean flat-slab: Journal of South American Earth Sciences, v. 15, p. 39–57, https://doi.org/10.1016/S0895-9811(02)00005-6.
- Keast, R.T., Brueseke, M.E., Trop, J.M., Berkelhammer, S.E., and Benowitz, J., 2016, Volcanic stratigraphy of the ~2.4 Ma Eucher Mountain volcano, Wrangell Arc, Alaska (U.S.A.): Geological Society of America Abstracts with Programs, v. 48, https://doi.org/10.1130/abs/2016AM-278627.
- Koehler, R.D., Farell, R., Burns, P.A.C., and Combellick, R.A., 2012, Quaternary faults and folds in Alaska: A digital database: Alaska Division of Geological & Geophysical Surveys Miscellaneous Publication 141, scale 1:3,700,000, 1 sheet, 31 p. text, https://doi.org/10.14509/23944.
- Lawton, T.F., 2008, Laramide sedimentary basins, in Miall, A.D., ed., The Sedimentary Basins of the United States and Canada: Amsterdam, Elsevier, p. 429–450.
- Lease, R.O., Haeussler, P.J., and O'Sullivan, P., 2016, Changing exhumation patterns during Cenozoic growth and glaciation of the Alaska Range: Insights from detrital thermochronology and geochronology: Tectonics, v. 35, p. 934–955, https://doi.org/10.1002/2015TC004067.
- Leat, P.T., Pearce, J.A., Barker, P.F., Millar, I.L., Barry, T.L., and Larter, R.D., 2004, Magma genesis and mantle flow at a subducting slab edge: The South Sandwich arc-basin system: Earth and Planetary Science Letters, v. 227, p. 17–35, https://doi.org/10.1016/j.epsl.2004.08.016.
- Lebrun, J.F., Lamarche, G., Collot, J.Y., and Delteil, J., 2000, Abrupt strike-slip fault to subduction transition: The Alpine fault-Puysegur trench connection, New Zealand: Tectonics, v. 19, p. 688–706, https://doi.org/10.1029/2000TC900008.
- Lee, H.Y., Chung, S.L., and Yang, H.M., 2016, Late Cenozoic volcanism in central Myanmar: Geochemical characteristics and geodynamic significance: Lithos, v. 245, p. 174–190, https://doi .org/10.1016/j.lithos.2015.09.018.
- Leeman, W.P., 2020, Old/new subduction zone paradigms as seen from the Cascades: Frontiers of Earth Science, v. 8, https://doi.org/10.3389/feart.2020.535879.
- Lerbekmo, J.F., 2008, The White River ash: largest Holocene Plinian tephra: Canadian Journal of Earth Sciences, v. 45, p. 693–700, https://doi.org/10.1139/E08-023.
- Li, S., Freymueller, J., and McCaffrey, R., 2016, Slow slip events and time-dependent variations in locking beneath Lower Cook Inlet of the Alaska-Aleutian subduction zone: Journal of Geophysical Research: Solid Earth, v. 121, p. 1060–1079.
- Llanes, P., Silver, E., Day, S., and Hoffman, G., 2009, Interactions between a transform fault and arc volcanism in the Bismarck Sea, Papua New Guinea: Geochemistry, Geophysics, Geosystems, v. 10, no. 6, https://doi.org/10.1029/2009GC002430.
- Lowey, G.W., 1998, A new estimate of the amount of displacement on the Denali fault system based on the occurrence of carbonate megaboulders in the Dezadeash Formation (Jura-Cretaceous), Yukon, and the Nutzotin Mountains sequence (Jura-Cretaceous), Alaska: Bulletin of Canadian Petroleum Geology, v. 46, p. 379–386.
- MacKevett, E.M., 1971, Stratigraphy and general geology of the McCarthy C-5 quadrangle, Alaska: U.S. Geological Survey Bulletin 1323, 35 p.

- Malusà, M.G., Resentini, A., and Garzanti, E., 2016, Hydraulic sorting and mineral fertility bias in detrital geochronology: Gondwana Research, v. 31, p. 1–19, https://doi.org/10.1016/j.gr .2015.09.002.
- Mann, M.E., Abers, G.A., Daly, K.A., and Christensen, D.H., 2020, High-resolution receiver function imaging of the subduction zone across south-central Alaska: Abstract T048–0009 presented at 2020 Virtual Fall Meeting, American Geophysical Union, 1–17 December.
- Manselle, P., Brueseke, M.E., Trop, J.M., Benowitz, J.A., Snyder, D.C., and Hart, W.K., 2020, Geochemical and stratigraphic analysis of the Chisana Formation, Wrangellia terrane, eastern Alaska: Insights into Early Cretaceous magmatism and tectonics along the northern Cordilleran margin: Tectonics, v. 39, no. e2020TC006131.
- Marechal, A., Ritz, J.F., Ferry, M., Mazzotti, S., Blard, P.H., Braucher, R., and Saint-Carlier, D., 2018, Active tectonics around the Yakutat indentor: New geomorphological constraints on the eastern Denali, Totschunda and Duke River faults: Earth and Planetary Science Letters, v. 482, p. 71–80, https://doi.org/10.1016/j.epsl.2017.10.051.
- Martinod, J., Husson, L., Roperch, P., Guillaume, B., and Espurt, N., 2010, Horizontal subduction zones, convergence velocity and the building of the Andes: Earth and Planetary Science Letters, v. 299, p. 299–309, https://doi.org/10.1016/j.epsl.2010.09.010.
- Maury, R.C., Pubellier, M., Rangin, C., Wulput, L., Cotten, J., Socquet, A., Bellon, H., Guillaud, J.P., and Htun, H.M., 2004, Quaternary calc-alkaline and alkaline volcanism in a hyper-oblique convergence setting, central Myanmar and western Yunnan: Bulletin de la Société Géologique de France, v. 175, p. 461–472, https://doi.org/10.2113/175.5.461.
- Milde, E.R., Fitzgerald, P.G., and Benowitz, J.A., 2013, Applying low-temperature thermochronology to constrain the tectonic history of the strike-slip Totschunda fault system, southeastern Alaska: Geological Society of America Abstracts with Programs, v. 45, no. 7, p. 163.
- Miller, T.P., McGimsey, R.G., Richter, D.H., Riehle, J.R., Nye, C.J., Yount, M.E., and Dumoulin, J.A., 1998, Catalog of the historically active volcanoes of Alaska: U.S. Geological Survey Open File Report 98-582, 104 p., https://doi.org/10.3133/ofr98582.
- Mortensen, J.K., and Hulbert, L.J., 1992, A U-Pb zircon age for a Maple Creek gabbro sill, Tata-magouche Creek area, southwestern Yukon Territory: Radiogenic Age and Isotopic Studies: Report 5: Geological Survey of Canada, Paper 91–2, p. 175–179.
- Morter, B.K., 2017, Understanding the history of a volcanic arc: Linking geochemistry of Cenozoic volcanic cobbles from the Wrangell arc, Alaska, to upper plate and subducting slab tectonic processes [M.S. thesis]: Manhattan, Kansas State University, http://hdl.handle.net /2007/38164
- Nelson, J., and Gehrels, G.E., 2007, Detrital zircon geochronology and provenance of the southeastern Yukon-Tanana terrane: Canadian Journal of Earth Sciences, v. 44, p. 297–316, https:// doi.org/10.1139/e06-105.
- Nie, J., Horton, B.K., Saylor, J.E., Mora, A., Mange, M., Garzione, C.N., Basu, A., Moreno, C.J., Caballero, V., and Parra, M., 2012, Integrated provenance analysis of a convergent retroarc foreland system: U–Pb ages, heavy minerals, Nd isotopes, and sandstone compositions of the Middle Magdalena Valley basin, northern Andes, Colombia: Earth-Science Reviews, v. 110, p. 111–126, https://doi.org/10.1016/j.earscirev.2011.11.002.
- Nye, C.J., 1983, Petrology and geochemistry of Okmok and Wrangell volcanoes, Alaska [Ph.D. thesis]: Santa Cruz, University of California, 208 p.
- Nye, C.J., Beget, J.E., Layer, P.W., Mangan, M.T., McConnell, V.S., McGimsey, R.G., Miller, T.P., Moore, R.B., and Stelling, P.L., 2018, Geochemistry of some Quaternary lavas from the Aleutian Arc and Mt. Wrangell: State of Alaska, Alaska Division of Geological & Geophysical Surveys, Raw Data File RDF 2018–1, https://doi.org/10.14509/29843.
- Park, J., Levin, V., Brandon, M., Lees, J., Peyton, V., Gordeev, E., and Ozerov, A., 2002, A dangling slab, amplified arc volcanism, mantle flow and seismic anisotropy in the Kamchatka plate corner, in Stein, S., and Freymueller, J.T., eds., Plate Boundary Zones: Washington, D.C., American Geophysical Union Monograph, v. 30, p. 295–324, https://doi.org/10.1029/GD030p0295.
- Paterson, S.R., Memeti, V., Anderson, L., Cao, W., Lackey, J.S., Putirka, K.D., Miller, R.B., Miller, J.S., and Mundil, R., 2014, Overview of arc processes and tempos, in Memeti, V., Paterson, S.R., and Putirka, K.D., eds., Formation of the Sierra Nevada Batholith: Magmatic and Tectonic Processes and Their Tempos: Geological Society of America Field Guide 34, p. 87–116, https://doi.org/10.1130/2014.0034(06).
- Pavlis, G.L., Bauer, M.A., Elliott, J.L., Koons, P., Pavlis, T.L., Ruppert, N., Ward, K.M., and Worthington, L.L., 2019, A unified three-dimensional model of the lithospheric structure at the subduction corner in southeast Alaska: Summary results from STEEP: Geosphere, v. 15, p. 382–406, https://doi.org/10.1130/GES01488.1.

- Pavlis, T.L., Chapman, J.B., Bruhn, R.L., Ridgway, K.D., Worthington, L.L., Gulick, S.P.S., and Spotila, J., 2012, Structure of the actively deforming fold-thrust belt of the St. Elias orogen with implications for glacial exhumation and three-dimensional tectonic processes: Geosphere, v. 8, p. 991–1019, https://doi.org/10.1130/GES00753.1.
- Pecha, M.E., Gehrels, G.E., McClelland, W.C., Giesler, D., White, C., and Yokelson, I., 2016, Detrital zircon U-Pb geochronology and Hf isotope geochemistry of the Yukon-Tanana terrane, Coast Mountains, southeast Alaska: Geosphere, v. 12, p. 1556–1574, https://doi.org/10.1130/GES01303.1.
- Plafker, G., and Berg, H.C., 1994, Overview of the geology and tectonic evolution of Alaska, in Plafker, G., and Berg, H.C., eds., The Geology of Alaska: Boulder, Colorado, Geological Society of America, The Geology of North America, v. G-1, p. 989–1021, https://doi.org/10.1130 /DNAG-GNA-G1989.
- Plafker, G., Nokleberg, W.J., and Lull, J.S., 1989, Bedrock geology and tectonic evolution of the Wrangellia, Peninsular, and Chugach terranes along the Trans-Alaska Crustal Transect in the Chugach Mountains and southern Copper River basin, Alaska: Journal of Geophysical Research: Solid Earth, v. 94, B4, p. 4255–4295, https://doi.org/10.1029/JB094iB04p04255.
- Plafker, G., Gilpin, L.M., and Lahr, J.C., 1994, Neotectonic map of Alaska, *in* Plafker, G., and Berg, H., eds., The Geology of Alaska: Geological Society of America, scale 1:2,500,000, 2 sheets.
- Polonia, A., Torelli, L., Brancolini, G., and Loreto, M.F., 2007, Tectonic accretion versus erosion along the southern Chile trench: Oblique subduction and margin segmentation: Tectonics, v. 26, no. 3, https://doi.org/10.1029/2006TC001983.
- Portnyagin, M., Horenle, K., Avdeiko, G., Hauff, F., Werner, R., Bindeman, I., Uspensky, V., and Garbe-Schönberg, D., 2005, Transition from arc to oceanic magmatism at the Kamchatka-Aleutian junction: Geology, v. 33, p. 25–28, https://doi.org/10.1130/G20853.1.
- Preece, S.J., and Hart, W.K., 2004, Geochemical variations in the <5 Ma Wrangell Volcanic Field, Alaska: Implications for the magmatic and tectonic development of a complex continental arc system: Tectonophysics. v. 392. p. 165–191. https://doi.org/10.1016/j.tecto.2004.04.011.
- Preece, S.J., McGimsey, R.G., Westgate, J.A., Pearce, N.J.G., Hart, W.K., and Perkins, W.T., 2014, Chemical complexity and source of the White River Ash, Alaska and Yukon: Geosphere, v. 10, p. 1020–1042, https://doi.org/10.1130/GES00953.1.
- Premo, W.R., Morton, D.M., Wooden, J.L., and Fanning, C.M., 2014, U-Pb zircon geochronology of plutonism in the northern Peninsular Ranges batholith, southern California: Implications for the Late Cretaceous tectonic evolution of southern California, in Morton, D.M., and Miller, Fk., Peninsular Ranges Batholith, Baja California and Southern California: Boulder, Colorado, USA, Geological Society of America Memoir 211, p. 145–180, https://doi.org/10.1130/2014.1211(04).
- Read, P.B., and Monger, J.W.H., 1976, Pre-Cenozoic volcanic assemblages of the Kluane and Alsek Ranges, southwestern Yukon Territory: Geological Survey of Canada Open-File Report 381, 96 p., https://doi.org/10.4095/129470.
- Regan, S.P., Benowitz, J.A., and Holland, M.E., 2020, A plutonic brother from another magma mother: Disproving the Eocene Foraker-McGonagall pluton piercing point and implications for long-term slip on the Denali fault: Terra Nova, v. 32, p. 66–74, https://doi.org/10.1111/ter.12437.
- Regan, S.P., Benowitz, J.A., Waldien, T.S., Holland, M.E., Roeske, S.M., O'Sullivan, P., and Layer, P., 2021, Long distance plutonic relationships demonstrate 33 million years of strain partitioning along the Denali fault: Terra Nova, v. 33, p. 630–640, https://doi.org/10.1111/ter.12555.
- Reid, M., Finzel, E.S., Enkelmann, E., and McClelland, W.C., 2018, Detrital zircon provenance of Upper Jurassic-Upper Cretaceous forearc basin strata on the Insular terranes, south-central Alaska, in Ingersoll, R.V., Lawton, T.F., and Graham, S.A., eds., Tectonics, Sedimentary Basins, and Provenance: A Celebration of William R. Dickinson's Career: Geological Society of America Special Paper 540, p. 1–20, https://doi.org/10.1130/2018.2540(25).
- Riccio, S.J., Fitzgerald, P.G., Benowitz, J.A., and Roeske, S.M., 2014, The role of thrust faulting in the formation of the eastern Alaska Range: Thermochronological constraints from the Susitna Glacier thrust fault region of the intracontinental strike-slip Denali fault system: Tectonics, v. 33, p. 2195–2217, https://doi.org/10.1002/2014TC003646.
- Richter, D.H., 1976, Geologic map of the Nabesna quadrangle: U.S. Geological Survey Miscellaneous Geologic Investigations Map I-932, scale 1:250,000, 1 sheet.
- Richter, D.H., Lanphere, M.A., and Matson, N.A., Jr., 1975, Granitic plutonism and metamorphism, eastern Alaska Range, Alaska: Geological Society of America Bulletin, v. 86, p. 819–829, https://doi.org/10.1130/0016-7606(1975)86<819:GPAMEA>2.0.CO;2.
- Richter, D.H., Smith, J.G., Lanphere, M.A., Dalrymple, G.B., Reed, B.L., and Shew, N., 1990, Age and progression of volcanism, Wrangell volcanic field, Alaska: Bulletin of Volcanology, v. 53, p. 29–44, https://doi.org/10.1007/BF00680318.

- Richter, D.H., Moll-Stalcup, E.J., Miller, T.P., Lanphere, M.A., Dalrymple, G.B., and Smith, R.L., 1994, Eruptive history and petrology of Mount Drum volcano, Wrangell Mountains, Alaska: Bulletin of Volcanology, v. 56, p. 29–46, https://doi.org/10.1007/BF00279727.
- Richter, D.H., Ratté, J.C., Leeman, W.P., and Menzies, M., 2000, Geologic map of the McCarthy D-1 quadrangle, Alaska: U.S. Geological Survey Geologic Investigations Series I-2695, scale 1:63,360, 1 sheet.
- Richter, D.H., Preller, C.C., Labay, K.A., and Shew, N.B., 2006, Geologic map of the Wrangell– Saint Elias Park and Preserve, Alaska: U.S. Geological Survey Scientific Investigations Map 2877, scale 1:350,000, 1 sheet, 15 p. text.
- Ridgway, K.D., and DeCelles, P.G., 1993, Stream-dominated alluvial-fan and lacustrine depositional systems in Cenozoic strike-slip basins, Denali fault system, Yukon Territory: Sedimentology, v. 40, p. 645–666, https://doi.org/10.1111/j.1365-3091.1993.tb01354.x.
- Ridgway, K.D., Thoms, E.E., Layer, P.W., Lesh, M.E., White, J.M., and Smith, S.V., 2007, Neogene transpressional foreland basin development on the north side of the central Alaska Range, Usibelli Group and Nenana Gravel, Tanana basin, in Ridgway, K.D., Trop, J.M., Glen, J.M.G., and O'Neill, J.M., eds., Tectonic Growth of a Collisional Continental Margin: Crustal Evolution of Southern Alaska: Geological Society of America Special Paper 431, p. 507–547, https://doi.org/10.1130/2007.2431(20).
- Rioux, M., Hacker, B., Mattinson, J., Kelemen, P., Blusztajn, J., and Gehrels, G., 2007, Magmatic development of an intra-oceanic arc: High-precision U-Pb zircon and whole-rock isotopic analyses from the accreted Talkeetna arc, south-central Alaska: Geological Society of America Bulletin, v. 119, p. 1168–1184, https://doi.org/10.1130/B25964.1.
- Roeske, S.M., Snee, L.W., and Pavlis, T.L., 2003, Dextral slip reactivation of an arc-forearc boundary during Late Cretaceous-early Eocene oblique convergence in the northern Cordillera, in Sisson, V.B., Roeske, S.R., and Pavlis, T.L., eds., Geology of a Transpressional Orogen Developed during Ridge-Trench Interaction along the North Pacific Margin: Geological Society of America Special Paper 371, p. 141–169, https://doi.org/10.1130/0-8137-2371-X.141.
- Rondenay, S., Montési, L.G., and Abers, G.A., 2010, New geophysical insight into the origin of the Denali volcanic gap: Geophysical Journal International, v. 182, p. 613–630, https://doi.org/10.1111/j.1365-246X.2010.04659.x.
- Schartman, A., Enkelmann, E., Garver, J.I., and Davidson, C.M., 2019, Uplift and exhumation of the Russell Fiord and Boundary blocks along the northern Fairweather transform fault, Alaska: Lithosphere, v. 11, p. 232–251, https://doi.org/10.1130/L1011.1.
- Schellart, W.P., 2017, Andean mountain building and magmatic arc migration driven by subduction-induced whole mantle flow: Nature Communications, v. 8, no. 2010, https://doi.org/10.1038/s41467-017-01847-z.
- Schellart, W.P., 2020, Control of subduction zone age and size on flat slab subduction: Frontiers of Earth Science, v. 8, p. 1–18.
- Skulski, T., Francis, D., and Ludden, J., 1991, Arc-transform magmatism in the Wrangell volcanic belt: Geology, v. 19, p. 11–14, https://doi.org/10.1130/0091-7613(1991)019<0011:ATMITW>2.3
- Skulski, T., Francis, D., and Ludden, J., 1992, Volcanism in an arc-transform transition zone: the stratigraphy of the St. Clare Creek volcanic field, Wrangell volcanic belt, Yukon, Canada: Canadian Journal of Earth Sciences, v. 29, p. 446–461, https://doi.org/10.1139/e92-039.
- Smith, J.G., and MacKevett, E.M., 1970, The Skolai Group in the McCarthy B-4, C-4, and C-5 quadrangles, Wrangell Mountains, Alaska: U.S. Geological Survey Bulletin, 1274-Q, scale 1:96,000, 1 sheet, p. Q1–Q26.
- Snyder, D.E., and Hart, W.K., 2007, The White Mountain granitoid suite: Isotopic constraints on source reservoirs for Cretaceous magmatism within the Wrangellia Terrane, in Ridgway, K.D., Trop, J.M., Glen, J.M.G., and O'Neill, J.M., eds., Tectonic Growth of a Collisional Continental Margin: Crustal Evolution of Southern Alaska: Geological Society of America Special Paper 431, p. 379–399, https://doi.org/10.1130/2007.2431(15).
- Spencer, C.J., Kirkland, C.L., and Roberts, N.M., 2018, Implications of erosion and bedrock composition on zircon fertility: Examples from South America and Western Australia: Terra Nova, v. 30, p. 289–295.
- Stevens Goddard, A.L., and Carrapa, B., 2018, Using basin thermal history to evaluate the role of Miocene–Pliocene flat-slab subduction in the southern Central Andes (27° S–30° S): Basin Research, v. 30, p. 564–585, https://doi.org/10.1111/bre.12265.
- Stevens Goddard, A.L., Trop, J.M., and Ridgway, K.D., 2018, Detrital zircon record of a Mesozoic collisional forearc basin in south central Alaska: The tectonic transition from an oceanic to continental arc: Tectonics, v. 37, p. 529–557, https://doi.org/10.1002/2017TC004825.

- Symeou, V., Homberg, C., Nader, F.H., Darnault, R., Lecomte, J.C., and Papadimitriou, N., 2018, Longitudinal and temporal evolution of the tectonic style along the Cyprus Arc system, assessed through 2-D reflection seismic interpretation: Tectonics, v. 37, p. 30–47, https://doi.org/10.1002/2017TC004667.
- Syracuse, E.M., and Abers, G.A., 2006, Global compilation of variations in slab depth beneath arc volcanoes and implications: Geochemistry, Geophysics, Geosystems, v. 7, no. 5, https://doi.org/10.1029/2005GC001045.
- Tait, L., Roeske, S., Mookerjee, M., Benowitz, J., and Huff, C.J., 2016, Heterogeneous Exhumation of mid-crustal rocks along the Hayes restraining bend of the central Denali fault: Abstract #T21D-2851 presented at 2016 Fall Meeting, American Geophysical Union, San Francisco, California, 12-16 December.
- Terhune, P.J., Benowitz, J.A., Trop, J.M., O'Sullivan, P.B., Gillis, R.J., and Freymueller, J.T., 2019, Cenozoic tectono-thermal history of the southern Talkeetna Mountains, Alaska: Insights into a potentially alternating convergent and transform plate margin: Geosphere, v. 15, p. 1539–1576, https://doi.org/10.1130/GES02008.1.
- Thorkelson, D.J., Madsen, J.K., and Sluggett, C.L., 2011, Mantle flow through the Northern Cordilleran slab window revealed by volcanic geochemistry: Geology, v. 39, p. 267–270, https://doi.org/10.1130/G31522.1.
- Tochilin, C., Gehrels, G., Nelson, J., and Mahoney, J.B., 2014, U-Pb and Hf isotope analysis of detrital zircons from the Banks Island assemblage (coastal British Columbia) and southern Alexander terrane (southeast Alaska): Lithosphere, v. 6, p. 200–215, https://doi.org/10.1130 /L338.1.
- Triplehorn, D.M., Drake, J., and Layer, P.W., 1999, Preliminary **a^Ar/**ages from two units in the Usibelli Group, Healy, Alaska: New light on some old problems, *in Pinney*, D.S., and Davis, P.K., eds.: Short Notes on Alaska Geology 1999: Alaska Division of Geological & Geophysical Surveys Professional Report 1191, p. 117–127.
- Trop, J.M., Hart, W.K., Snyder, D., and Idleman, B., 2012, Miocene basin development and volcanism along a strike-slip to flat-slab subduction transition: Stratigraphy, geochemistry, and geochronology of the central Wrangell volcanic belt, Yakutat-North America collision zone: Geosphere, v. 8, p. 805–834, https://doi.org/10.1130/GES00762.1.
- Trop, J.M., Benowitz, J.A., Cole, R., and O'Sullivan, P., 2019, Cretaceous to Miocene magmatism, sedimentation, and exhumation within the Alaska Range suture zone: A reactivated terrane boundary: Geosphere, v. 15, p. 1066–1101, https://doi.org/10.1130/GES02014.1.
- Trop, J.M., Benowitz, J.A., Koepp, D.Q., Sunderlin, D., Brueseke, M.E., Layer, P.W., and Fitzgerald, P.G., 2020, Stitch in the ditch: Nutzotin Mountains (Alaska) fluvial strata and a dike record ca. 117–114 Ma accretion of Wrangellia with western North America and initiation of the Totschunda fault: Geosphere, v. 16, p. 82–110, https://doi.org/10.1130/GES02127.1.
- Trumbull, R.B., Riller, U., Oncken, O., Scheuber, E., Munier, K., and Hongn, F., 2006, The time-space distribution of Cenozoic volcanism in the South-Central Andes: A new data compilation and some tectonic implications, in Oncken, O., Chong, G., Franz, G., Giese, P., Götze, H.-J., Ramos, V.A., Strecker, M.R., and Wigger, P., eds., The Andes, Frontiers in Earth Sciences: Berlin, Heidelberg, Springer, p. 29–43, https://doi.org/10.1007/978-3-540-48684-8_2.
- van der Heyden, P., 1992, A Middle Jurassic to early Tertiary Andean-Sierran arc model for the Coast belt of British Columbia: Tectonics, v. 11, p. 82–97, https://doi.org/10.1029/91TC02183.
- Wakabayashi, J., 1996, Tectono-metamorphic impact of a subduction-transform transition and implications for interpretation of orogenic belts: International Geology Review, v. 38, p. 979– 994, https://doi.org/10.1080/00206819709465376.
- Waldien, T.S., Roeske, S.M., and Benowitz, J.A., 2018a, The effects of superimposed deformation events on strike-slip translation in the Cordillera: An example from the Denali fault system: Geological Society of America Abstracts with Programs, v. 50, no. 5, https://doi.org/10.1130 /abs/2018RM-313929.
- Waldien, T.S., Roeske, S.M., Benowitz, J.A., Allen, W.K., Ridgway, K.D., and O'Sullivan, P.B., 2018b, Late Miocene to Quaternary evolution of the McCallum Creek thrust system, Alaska: Insights for range-boundary thrusts in transpressional orogens: Geosphere, v. 14, p. 2379–2406, https://doi.org/10.1130/GES01676.1.
- Waldien, T.S., Roeske, S.M., Benowitz, J.A., Twelker, E., and Miller, M.S., 2021, Oligocene–Neogene lithospheric-scale reactivation of Mesozoic terrane accretionary structures in the Alaska Range suture zone, southern Alaska, USA: Geological Society of America Bulletin, v. 133, p. 691–716, https://doi.org/10.1130/B35665.1.
- Wang, B., Cluzel, D., Shu, L., Faure, M., Charvet, J., Chen, Y., Meffre, S., and de Jong, K., 2009, Evolution of calc-alkaline to alkaline magmatism through Carboniferous convergence to

- Permian transcurrent tectonics, western Chinese Tianshan: International Journal of Earth Sciences, v. 98, p. 1275–1298, https://doi.org/10.1007/s00531-008-0408-y.
- Weber, M.A., Brueseke, M.E., Berkelhammer, S.E., Benowitz, J.A., Trop, J.M., Davis, K.N., Layer, P.W., and Morter, B.K., 2017, Geochemical evidence for adakite-like magmatism at the Oligo– Miocene initiation of the Wrangell arc, Alaska: Geological Society of America Abstracts with Programs, v. 49, no. 6, https://doi.org/10.1130/abs/2017AM-303842.
- White, C., Gehrels, G., Pecha, M., Giesler, D., Yokelson, I., McClelland, W., and Butler, R., 2016, U-Pb and Hf isotope analysis of detrital zircons from Paleozoic strata of the southern Alexander terrane (southeast Alaska): Lithosphere, v. 8, p. 83–96, https://doi.org/10.1130/L475.1.
- Willeit, M., Ganopolski, A., Calov, R., and Brovkin, V., 2019, Mid-Pleistocene transition in glacial cycles explained by declining CO₂ and regolith removal: Science Advances, v. 5, no. eaav7337, https://doi.org/10.1126/sciadv.aav7337.
- Wilson, A.M., and Russell, J.K., 2020, Glacial pumping of a magma-charged lithosphere: A model for glaciovolcanic causality in magmatic arcs: Earth and Planetary Science Letters, v. 548, no. 116500, https://doi.org/10.1016/j.epsl.2020.116500.

- Wilson, F.H., Hults, C.P., Mull, C.G., and Karl, S.M., compilers, 2015, Geologic map of Alaska: U.S. Geological Survey Scientific Investigations Map 3340, scale 1:1,584,000, 2 sheets, 204 p. text.
- Worthington, L.L., Van Avendonk, H.J., Gulick, S.P., Christeson, G.L., and Pavlis, T.L., 2012, Crustal structure of the Yakutat terrane and the evolution of subduction and collision in southern Alaska: Journal of Geophysical Research: Solid Earth, v. 117, https://doi.org/10.1029 /2011JB008493.
- Yang, X., and Gao, H., 2020, Segmentation of the Aleutian-Alaska subduction zone revealed by full-wave ambient noise tomography: Implications for the along-strike variation of volcanism: Journal of Geophysical Research: Solid Earth, v. 125, no. e2020JB019677, https://doi.org/10 .1029/2020JB019677.
- Yokelson, I., Gehrels, G.E., Pecha, M., Giesler, D., White, C., and McClelland, W.C., 2015, U-Pb and Hf isotope analysis of detrital zircons from Mesozoic strata of the Gravina belt, southeast Alaska: Tectonics, v. 34, p. 2052–2066, https://doi.org/10.1002/2015TC003955.
- Yukon Geological Survey, 2020, Bedrock geology map index: http://data.geology.gov.yk.ca/Compilation/34.